The science of brown dwarfs

Adam Burrows

Departments of Physics and Astronomy, University of Arizona, Tucson, Arizona 85721

James Liebert

Department of Astronomy and Steward Observatory, University of Arizona, Tucson, Arizona 85721

This review summarizes the current status of both brown dwarf theory and the searches for these elusive substellar objects. The conceptual continuity between the brown dwarf and the well-studied M dwarf branches is emphasized throughout. The physics of their atmospheres and interiors is reviewed and an analytic model of both brown dwarf evolution and the lower edge of the hydrogen main sequence is presented. An extensive discussion of brown dwarf searches in the field, in binaries, around white dwarfs, in clusters, in the solar neighborhood, in the galactic halo, and using proper-motion catalogs is provided, as is a tentative list of candidates in the field. The theory near and below the edge of the main sequence, while sophisticated, is only now being successfully challenged by optical and infrared observations. The near future promises a productive explosion in our knowledge of this problematic galactic population.

CONTENTS

As one great furnace flamed, yet from those flames
No light, but rather darkness visible.

Milton—Paradise Lost

Nothing is secret which shall not be made manifest.

Luke 8:17

I. INTRODUCTION

Between giant planets such as Jupiter ($\sim 10^{-3}M_{\odot}$) and stars at the bottom of the hydrogen main sequence ($\lesssim 0.1M_{\odot}$), the galactic census is woefully incomplete. Spanning two orders of magnitude in mass, this *brown dwarf* branch (Tarter, 1975, 1986) is all but unexplored, yet may contain the majority of objects in the galactic disk and halo. That there is a minimum mass for stable hydrogen burning ($\sim 0.08M_{\odot}$), and, hence, that there is a lower edge to the stellar branch, has been known theoretically since the pioneering work of Kumar (1963). However, no credible arguments have been advanced for why the edge of the main sequence should be the edge of the "stellar" mass function. Brown dwarfs emit most of their energy in the near infrared and can cool quickly below the luminosity of $\sim 10^{-4}L_{\odot}$ at the main-sequence edge. Nevertheless, the brown dwarf branch should be populated, and realistic extrapolations from the adjacent M dwarf branch simply an abundance. However, if brown dwarfs are so numerous, why have we no unambiguous examples? This question cannot yet be answered, but it is now being posed with more and more vigor as new infrared technology is applied to the search. Paralleling the increased observational activity has been the increased theoretical interest. These transition objects, which straddle the realms of planets and stars, are made

predominantly of liquid metallic hydrogen, have "razor-thin" atmospheres composed of an exotic soup of molecules and grains, and can achieve central temperatures adequate to consume their stores of cosmological deuterium, while inadequate to ignite sufficient light hydrogen to avoid cooling into obscurity within a Hubble time.

For background material on the general theory of stellar evolution and compact objects, the inquisitive will find the books by Clayton (1983), Shapiro and Teukolsky (1983), Hubbard (1984), and Chandrasekhar (1939) profitable reading. Though we do not here attempt to include any discussion of the current theories of star formation, the articles by Zinnecker, McCaughrean, and Wilking (1992), Shu, Adams, and Lizano (1987), and Boss (1987) will serve as useful introductions to that annoyingly incomplete subject.

This review is meant to combine the latest theoretical thinking with the latest observations in a state-of-the-art snapshot of brown dwarf science. We are not motivated by any prejudice that brown dwarfs might be the "missing mass" of the galactic disk (if there is such a mass) or of the galactic halo. Rather, we are driven by the lure of one of the last terrae incognitae in astronomy.

Section II deals with the theory of brown dwarf structure and cooling. It contains not only a useful analytic model, but detailed numerical models as well. Brown dwarf atmospheres are described and a comprehensive equation of state is presented, along with an informative, if crude, analytic calculation of the mass at the main-sequence edge. Section III surveys the various searches and classes of searches. Highlighted are investigations in proper-motion catalogs, and the searches in the field, in binaries, around white dwarfs, in clusters, in the solar neighborhood, and in the galactic halo. The samples in which mass, age, and/or distance are known are reviewed, and a current brown dwarf candidate list is presented. Throughout, the continuity between the M dwarf and the brown dwarf branches is emphasized. However, as Sec. III demonstrates, the comparison between a theory that deals with effective temperatures and bolometric luminosities, and observations that involve photometric colors and magnitudes, is handicapped by the lack of good theoretical color-color and color-magnitude relations. Despite this problem, the brown dwarf candidate list continues to grow and scientific questions concerning the lower edge of the main sequence remain as interesting and challenging as ever.

II. THE PHYSICS OF BROWN DWARFS

Despite the small sample of candidate brown dwarfs from the optical and infrared surveys conducted to date (Sec. III), the theorists have not been idle [D'Antona and Mazzitelli, Nelson, Rappaport, and Joss, 1985, 1986a, 1986b, 1986c; Stringfellow, 1986; Burrows, Hubbard, and Lunine, 1989; Stringfellow, Black, and Bodenheimer, 1990; Burrows, Hubbard, Saumon, and Lunine, 1993]. The brown dwarf branch is the low-mass extension of the much-studied very-low-mass (VLM); $M \leq 0.3 M_{\odot}$) and low-mass ($M \leq 0.7 M_{\odot}$) stellar branches and as such should involve merely extrapolations in the equation of state (EOS), atmospheric physics, structure, and evolution appropriate for lighter and cooler objects.

Brown dwarfs are compact "stars," predominantly of hydrogen, that are not massive enough ($M \lesssim 0.08 M_{\odot}$) eventually to ignite hydrogen stably on the hydrogen main sequence. This is not to say that brown dwarfs do not burn hydrogen during some phase of their lives. In fact, the most massive ($M \gtrsim 0.07 M_{\odot}$) can burn hydrogen for billions of years. However, in a brown dwarf the nuclear fires are eventually extinguished as it cools to obscurity, and the surface energy losses are never completely compensated by thermonuclear burning in the core. The surface and central temperatures are never stabilized.

There is an unspoken prejudice in the cognizant community that "brown dwarfs" are formed (if formed at all) from the interstellar medium (ISM)—as are regular stars—and not in proto-planetary disks—as are giant planets. Brown dwarfs would then be aborted stars. The distinction between giant planets, such as Jupiter, and brown dwarfs is largely semantic, not physical, and at times objects between $10 M_J$ ($M_J \cong 0.001 M_{\odot}$) and $80 M_J$ are arbitrarily designated as brown dwarfs. Here, we need not be so narrow-minded, but the reader should be aware that there may be virtue in distinguishing objects with the same mass, but different origins.

In Sec. II, we address the scientific ingredients that must go into a complete theoretical attack on brown dwarfs. The theory that we describe assumes that brown dwarfs are formed, as are stars, from the cores of molecular clouds, that they accrete mass for no more than $\sim 10^5 - 10^6$ yr, and that they can be treated as spheres. Fortunately, these assumptions are minimal, and such objects forget their initial conditions quickly ($\leq 10^5 - 10^6$ yr). An important assumption that we have made in order to focus the presentation is that the metallicity of our theoretical objects is solar ($\sim 2\%$ by mass). This need not be the case, and we refer to Burrows *et al.* (1993) and D'Antona (1987) for a discussion of nonsolar models. For the theory of substellar objects that may accrete mass over a good fraction of a Hubble time, we refer the reader to Salpeter (1992).

Section II.A contains a general discussion of the "polytropic" nature and structure of brown dwarfs, and this is followed in Sec. II.B by a short primer on the relevant thermodynamics and equations of state. In Sec. II.C, the sources of atmospheric opacity and the physics of the outer radiative skin are reviewed. Section II.D deals with the thermonuclear rates and screening corrections that are important in the physics both above and just below the edge of the main sequence. In order to more clearly highlight the essentials of brown dwarf theory, Sec. II.E provides an analytic model for the time and mass dependences of the effective temperature (T_e) and the bolometric luminosity (L) along the entire brown dwarf branch. That section also contains an analytic

derivation of the value of the main-sequence transition mass. Finally, in Sec. II.F we present representative results from detailed numerical simulations, both unpublished and published, of brown dwarf properties and evolution. Throughout this review, we have relied heavily upon the insights and numbers to be culled from the broad literature. However, for practical reasons, we have drawn on the theory of Burrows, Hubbard, and Lunine (BHL) when the results of the numerical simulations were required. This habit is not meant to detract in any way from the important work of Grossman *et al.* (1974), Vandenberg *et al.* (1983), D'Antona and Mazzitelli (1985), Rappaport and Joss (1984), Nelson, Rappaport, and Joss (1986a, 1986b, 1986c), Dorman, Nelson, and Chou (1989), or Stringfellow (1986); and the reader is strongly encouraged to refer to these papers for an alternative view of the theoretical terrain.

A. The polytropic essentials of brown dwarf theory

Composed predominantly of metallic hydrogen and helium and with mass densities in the vicinity of 10–1000 gm/cm^3, brown dwarfs are supported in hydrostatic equilibrium by electron degeneracy pressure. It is only for a brief time ($\leq 10^8$ yr), early in their cooling-regulated contraction, when the central densities are sufficiently low and entropies are sufficiently high, that thermal ideal-gas pressure is important. But no matter the character of the pressure support, since a brown dwarf contracts along a Hayashi track, it is at all times convective (but for a *caveat,* see Nelson, Rappaport, and Joss, 1986a). This implies that the entropy is the same throughout the star (save for in the very thin outer radiative skin) and that the P-ρ relation is approximately a power law:

$$P = K'\rho^{1+1/n} \tag{2.1}$$

$$= K'\rho^{5/3} \quad (n = 1.5) , \tag{2.2}$$

where P is the pressure, ρ is the mass density, n is the polytropic index, and K' is a constant that in Eq. (2.2) depends only on the composition and the specific entropy. Stars that satisfy Eq. (2.1) are called polytropes of index n. (Note that it is the nonrelativistic nature of the pressure support that sets $n = 1.5$.) They form a sequence of objects with self-similar structure and radii (R), central densities (ρ_c), and central pressures (P_c) that depend on one another and on K' and M (the total mass) via simple power laws. The general equations of hydrostatic equilibrium

$$\frac{dP}{dr} = -\frac{GM(r)\rho}{r^2} , \tag{2.3}$$

$$\frac{dM(r)}{dr} = 4\pi r^2 \rho , \tag{2.4}$$

where G is Newton's universal constant of gravitation ($G = 6.6726 \times 10^{-8}$ cgs), can be combined for polytropes to yield the Lane-Emden equation (Chandrasekhar, 1939),

$$\frac{1}{\xi^2}\frac{d}{d\xi}\left[\xi^2 \frac{d\theta}{d\xi}\right] = -\theta^n, \quad \theta(0) = 1, \quad \left.\frac{d\theta}{d\xi}\right|_{\xi=0} = 0 , \tag{2.5}$$

where

$$\rho = \rho_c \theta^n, \quad P = P_c \theta^{n+1} \tag{2.5a}$$

and

$$\xi = \frac{r}{a}, \quad a = \left[(n+1)\frac{K'}{4\pi G}\rho_c^{(1-n)/n}\right]^{1/2} . \tag{2.5b}$$

The solution of Eq. (2.5) for $\theta(\xi)$ subject to the zero-pressure outer boundary condition solves the problem given ρ_c, K', and n or M, K', and n. Useful results are

$$\rho_c = \delta_n \langle \rho \rangle = \delta_n \left[\frac{3M}{4\pi R^3}\right] \propto M^{2n/(3-n)} , \tag{2.6}$$

$$P_c = W_n \frac{GM^2}{R^4} \propto M^{2(1+n)/(3-n)} , \tag{2.7}$$

and

$$R = \gamma_n \left[\frac{K'}{G}\right]^{n/(3-n)} M^{(1-n)/(3-n)} , \tag{2.8}$$

where δ_n, W_n, and γ_n are functions of n alone. For $n = 1.5$, $\delta_n = 5.991$, $W_n = 0.770$, and $\gamma_n = 2.357$ and, importantly, $\rho_c \propto M^2$, $P_c \propto M^{10/3}$, and $R \propto M^{-1/3}$. For $n = 1.0$, $\delta_n = \pi^2/3 = 3.29$, $W_n = 0.393$, and $\gamma_n = \sqrt{\pi/2} = 1.253$, while $\rho_c \propto M$, $P_c \propto M^2$, and R is independent of M.

At the low-mass end of the brown dwarf branch, for $M \lesssim 4M_J$, the Coulomb corrections to the P-ρ law compete with the degeneracy component and shift the effective polytropic index from 1.5 [Eq. (2.2)] for the more massive brown dwarfs to 1.0. As stated above, when $n = 1.0$, the radius of the object is independent of the mass. Figure 1, which schematically compares R versus M for cold brown dwarfs, M dwarfs, white dwarfs, and neutron stars, demonstrates that the radii of low-mass brown dwarfs plateau over a broad range of masses. Indeed, even above $M \cong 5M_J$ when $n \sim 1.5$ and $R \propto M^{-1/3}$, the dependence of the brown dwarf's radius on mass is weak. Zapolsky and Salpeter (1969) have provided a useful analytic fit to the radius-mass relation that includes both planets and cold brown dwarfs:

$$R = 2.2 \times 10^9 \left[\frac{M_\odot}{M}\right]^{1/3} \Big/ \left[1 + \left[\frac{M}{0.0032 M_\odot}\right]^{-1/2}\right]^{4/3} \text{cm} . \tag{2.9}$$

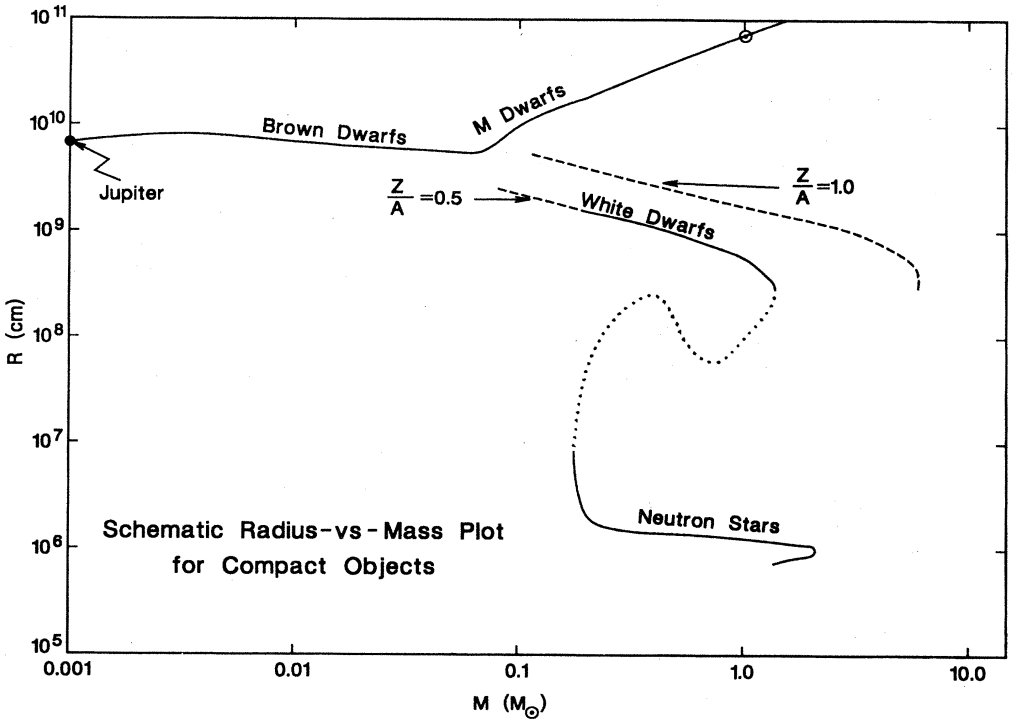

FIG. 1. Radius-mass plots for the variety of compact objects with surfaces. Depicted are the brown dwarf and M dwarf branches, the white dwarf branch ($Z/A=0.5$), and the unstable branch between white dwarfs and neutron stars. Shown too, is the high-mass continuation of the cold, pure hydrogen brown dwarf ($Z/A=1.0$) sequence. The positions of the Sun and Jupiter are clearly marked. See text for discussion.

In fact, as the mass ranges from M_J to $\sim 80M_J$ along the full cold brown dwarf branch, the radius changes by no more than 50% and is always near R_J ($=8.26\times10^9$ cm$\sim 0.12R_\odot$). Furthermore, in a structural, but not an evolutionary sense, cold brown dwarfs are at the hydrogen-rich (high Z/A), low-mass end of the white dwarf family.

Equations (2.6)–(2.8) allows us to derive most of the salient features of cold brown dwarfs. Their R's are near $0.1R_\odot$; ρ_c ranges from ~ 10 gm/cm^3 for the light to 1000 gm/cm^3 for the heavy; and P_c can be found above, near, and below 10^5 Mbar (1 Mbar$=10^{12}$ dyn/cm^2). However, the polytropic analysis alone does not illuminate the thermal structure and evolution of a brown dwarf. The time dependence of brown dwarf characteristics is a crucial dimension in brown dwarf theory. The effective photospheric temperature, luminosity, and central temperature (T_c) at a given time require a knowledge of the specific heat, atmospheric opacities, phases, etc. that cannot be extracted from Eqs. (2.1)–(2.8). Supplemented with this ancillary knowledge, the polytropic approximation can indeed provide an analytic model of brown dwarf theory (versus M and t). Stevenson (1991) and Rappaport and Joss (1984), in particular, have developed such models, and we provide our own version in Sec. II.E. However, an accurate theory must incorporate the thermodynamic and atmospheric details. The analytic model reveals the systematics, but only the full simulations should be used for numbers.

B. The equation of state and thermodynamics of hydrogen

More than 50 years ago, Wigner and Huntington (1935) postulated that under high pressures molecular hydrogen would undergo a phase transition to the metallic state. This metal-insulator transition has received sporadic attention ever since and is now the subject of an intense, but still ambiguous, experimental quest (Mao and Hemley, 1989; Mao, Hemley, and Hanfland, 1990; Van Horn, 1991). Nevertheless, the pressure ionization and metallization of hydrogen and hydrogen/helium mixtures is unavoidable, given suitable pressure ($P\gtrsim 3$ Mbar), and such an alloy must form the bulk of Jupiter ($\sim 85\%$), Saturn ($\sim 50\%$), and brown dwarfs ($>99.9\%$). Theoretical treatments of the thermodynamics and energetics of such strongly coupled Coulomb plasmas in astrophysical contexts have been attempted by many, but for this synopsis we have been guided by the work of Stevenson (1976, 1978, 1979, 1982, 1983, 1991). DeWitt and Hubbard (1976), Slattery, Doolen, and DeWitt (1982), Marley and Hubbard (1988), Magni and Mazzitelli (1979), Stringfellow, DeWitt, and Slattery (1990), Mestel and Ruderman (1967), and Saumon and Chabrier (1989), to any and all of which the reader is referred for details. Saumon and Chabrier, in particular, have provided a most careful theoretical treatment of pure hydrogen above and below the plasma phase transition (PPT), at high and low temperatures, and in the molecular,

atomic, and ionized state. A revealing temperature-density phase diagram for pure hydrogen inspired by Saumon and Chabrier (1989; Saumon, 1990) is shown in Fig. 2. This figure depicts most of the essential information concerning the thermodynamics of the entire brown dwarf and giant-planet family. Similar phase diagrams can be found in Stevenson (1991) and Hubbard (1984). A Jupiter (J) and two $0.05M_\odot$ brown dwarf adiabats (Burrows, Hubbard, and Lunine, 1989) are shown in Fig. 2 as dotted lines. Though these adiabats assume a helium mass fraction (Y_α) of 25% (for the dwarf) and 22% (for Jupiter), their superposition on a pure hydrogen phase diagram still makes for a fruitful comparison. The ×'s on these lines mark the points interior to which lie 50% of the object's mass. As is apparent, only a small mass fraction of these objects inhabits the low-temperature, low-density regime, while most of their mass is indeed in the liquid metallic state.

1. The low-density regime

Referring to the bottom left of Fig. 2, we note that at low densities (10^{-5} gm/cm^3 $<\rho<0.1$ gm/cm^3) and low temperatures ($T\lesssim 4000$ K) hydrogen is predominantly in the molecular state and is a fluid. Between ~ 0.1 and ~ 1.0 gm/cm^3 and far below the critical point (at $P_{\rm crit}=0.614$ Mbar, $T_{\rm crit}=1.53\times 10^4$ K, and $\rho_{\rm crit}=0.35$ gm/cm^3, marked "SC"), hydrogen is a solid. The solid-fluid transition is indicated with a dashed line. It should be emphasized again that the precise phase boundaries and details throughout the ρ-T plane are still a subject of debate (cf. Marley and Hubbard, 1988; Robnik and Kundt, 1983) and that, though the discussion here revolves around the Saumon and Chabrier equation of state, the subject is still in a state of productive flux.

As the temperature increases above $\sim 10^4$ K, molecular hydrogen first dissociates and then ionizes. Temperature ionization does not occur via a phase transition. At low densities and high temperatures, hydrogen is a very weakly coupled gas. The pressure law throughout the low-density regime is given approximately by the ideal-gas law

$$P=\frac{\rho N_A kT}{\mu}\ , \tag{2.10}$$

where N_A is Avogadro's number, k is Boltzmann's constant, and μ is the mean "molecular" weight. When hydrogen and helium are completely ionized (ignoring, for the moment, "metals"),

$$\frac{1}{\mu}=2X+\frac{3}{4}Y_\alpha\ ; \tag{2.11}$$

but when they are in the molecular state,

$$\frac{1}{\mu}=\frac{X}{2}+\frac{Y_\alpha}{4}\ , \tag{2.12}$$

where X and Y_α are the hydrogen and helium mass fractions, respectively. For $X=0.75$ and $Y_\alpha=0.25$, $\mu=0.593$ and 2.29 in the two regimes, but it is always of order unity.

The photosphere of a brown dwarf is located approximately at the $\tau=\frac{2}{3}$ surface, where τ is the optical depth given by

$$\tau=\int_r^\infty \kappa_R\rho\ dr\ . \tag{2.13}$$

κ_R is the Rosseland mean opacity. Using the equation of hydrostatic equilibrium (2.3) and (2.13), we obtain

$$P_e\cong\frac{2}{3}\frac{g}{\kappa_R}\sim 10^7\ {\rm dyn/cm^2}\equiv 10\ {\rm bars}\ , \tag{2.14}$$

where P_e is the pressure at the photosphere, g is the surface gravity and has been set equal to 10^5 cm/s^2, and κ_R has been set equal to 10^{-2} cm^2/g.

In a region such as the photosphere where it can be assumed that g is constant, Eqs. (2.3) and (2.4) can be rewritten as

$$\Delta M=\frac{4\pi R^2}{g}P\ , \tag{2.15}$$

where ΔM is the total mass that overlies the shell at pressure P and R is the total brown dwarf radius. Setting $P=P_e$, we derive that $\Delta M_{\rm Ph}\sim 10^{-11}M_\odot$. In addition, the polytropic Eq. (2.7) can be used to give us

$$\frac{\Delta M}{M}=[4\pi W_n]\frac{P}{P_c}\ , \tag{2.16}$$

where P_c is the central pressure and M is the total stellar mass. Of course, Eq. (2.16) gives us $\Delta M_{\rm Ph}/M\sim 10^{-10}$. The radiative region of a brown dwarf is indeed a prodigiously small fraction of the object.

Equation (2.10) implies that, at a photospheric temperature of ~ 1500 K, $\rho_e\sim 10^{-4}$ gm/cm^3 and puts the photosphere squarely in the gaseous molecular hydrogen region of Fig. 2. In and around this low-density, low-temperature region, the temperatures are sufficient to excite the rotational levels of the H_2 molecule into equipartition, but not its vibrational levels. This fact implies that the adiabatic indices ($\Gamma_1,\Gamma_2,\Gamma_3$) are all near $\frac{7}{5}$ ($=1.4$), not $\frac{5}{3}$. Therefore $P\propto\rho^{1.4}$ and $T\propto\rho^{0.4}$ along an adiabat. The shallow slopes of the brown dwarf adiabats in the low-density molecular region of Fig. 2 are a consequence of this rotational softening.

2. The high-density regime

Most of a brown dwarf can be found on the right-hand side of Fig. 2 in the high-density, liquid metallic region. Saumon and Chabrier adopt a "chemical picture" in which the actors (H, H_2, H^+, and e^-) interact via pair potentials. They identify a first-order plasma phase transition (PPT) that occurs over a narrow range of densities near 1.0 gm/cm^3 (shown as the hatched region in Fig. 2) and they conclude that molecular dissociation and pressure ionization concur. The transition is from a neutral phase ($X_e<10^{-3}$) to a partially ionized phase ($X_e\sim 0.5$)

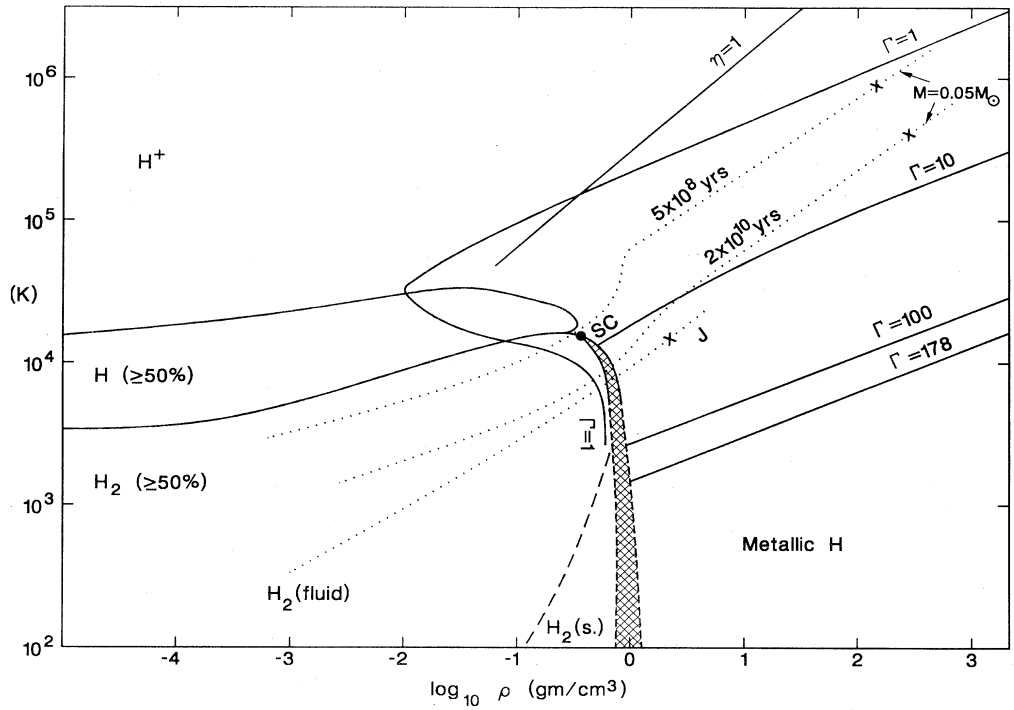

FIG. 2. Phase diagram of temperature (in K) vs density (in gm/cm^3) for pure hydrogen. Superposed as dotted curves are two $0.05M_\odot$, $Y_\alpha=0.25$ brown dwarf adiabats from BHL at 5×10^8 and 2×10^{10} yr and a Jupiter (J) adiabat. The $\times$'s on these adiabats mark the 50% mass point. Lines of constant Coulomb parameter (Γ) are provided, as is the $\eta=1$ line (see text). Shown clockwise are the solid H_2, liquid and gaseous H_2, atomic H, ionized H^+, and metallic H states. "SC" marks the critical point as calculated in Saumon and Chabrier (1989), to which one is referred for further details. The hatched region represents schematically the realm of the first-order plasma phase transition (PPT). See text for discussion.

and is at a pressure of 1–3 Mbar. Above the PPT, the ionization fraction increases rapidly with ρ to 1.0.

The characteristics of a strongly coupled Coulomb plasma are determined by the dimensionless Coulomb parameter, the ratio of the Coulomb energy per ion to kT:

$$\Gamma=\frac{Z^2e^2}{r_skT}=0.227\left[\frac{\rho}{\mu_e}\right]^{1/3}Z^{5/3}/T_6\ , \tag{2.17}$$

where Ze is the ionic charge ($Z=1$ for H), $T_6=T/10^6$ K, ρ is in cgs, and μ_e is the number of baryons per electron given by

$$\frac{1}{\mu_e}=X+\frac{1}{2}Y_\alpha=\frac{1+X}{2}\ . \tag{2.18}$$

For $Y_\alpha=0.25$, $\mu_e=1.143$. r_s is the radius of a sphere that contains one nucleus on average and, along with r_e, the electron spacing parameter, is the relevant length scale. r_s and r_e are defined as

$$r_s=\left[\frac{3Z}{4\pi n_e}\right]^{1/3}=\left[\frac{3\mu_eZ}{4\pi N_A\rho}\right]^{1/3} \tag{2.19}$$

and

$$r_e=\left[\frac{3}{4\pi n_e}\right]^{1/3}=\left[\frac{3\mu_e}{4\pi N_A\rho}\right]^{1/3}=\frac{r_s}{Z^{1/3}}\ , \tag{2.20}$$

where n_e is the electron density ($n_e=\rho N_A/\mu_e$). The weakly coupled regime is characterized by $\Gamma\ll1$ and is called the Debye-Hückel limit. This regime is encountered in both the Sun and in blood plasma. The transition to the strongly coupled liquid state occurs at $\Gamma\sim1$. As Fig. 2 implies, brown dwarf matter lies between $\Gamma\sim1$ and 10 in the liquid metal regime. Note that Γ in a brown dwarf achieves its *minimum* at its center and gradually grows to its highest value at or near the PPT.

Calculations of the thermodynamic properties of strong-coupled Coulomb plasmas have occupied many workers over the years and have achieved great sophistication (Hansen, 1973; Ichimaru, 1982; Hubbard and DeWitt, 1985; Ogata and Ichimaru, 1987; Spruch, 1991; Stevenson, 1991). One needs to include not only the simple Coulomb part of the ion-ion interaction, but also the electron exchange and correlation terms. Furthermore, electron screening and density-fluctuation corrections are required. Some of the various approaches that have been used in the past include the Wigner-Seitz approximation, the Thomas-Fermi-Dirac theory, and dielectric function theory. The latter, in particular, which focuses on the dielectric response of the plasma to calculate the effect of fluctuations in n_e on the Coulomb binding, has been quite fruitful (Hubbard and DeWitt, 1985). Since it will take us too far afield to describe the details of the physics of strongly coupled plasmas, we shall not do so here. How-

ever, some of the essentials that touch directly on brown dwarf theory bear mentioning.

The atomic unit of pressure ($P_0 = e^2/a_0^4$, where a_0 is the Bohr radius) is 294 Mbar. For pressures significantly above P_0, the degeneracy pressure of free electrons dominates and $P \sim P_D$ where

$$P_D \simeq 10^{13} \left[\frac{\rho}{\mu_e}\right]^{5/3} \frac{\text{dyn}}{\text{cm}^3} = 10 \text{ Mbar} \left[\frac{\rho}{\mu_e}\right]^{5/3} . \quad (2.21)$$

This echoes the polytropic form of Eq. (2.1) with $n = 1.5$. The temperature corrections to P are generally small along brown dwarf tracks (the electron component is especially small) and can be approximated by the Grüneisen (1926) theory:

$$P_T = \gamma E_T = \frac{3\gamma N_A kT}{V} , \quad (2.22)$$

where γ is the Grüneisen parameter [$0.6 \rightarrow 0.5$ for H from 1 to 10^6 Mbar (Hubbard, 1984)], E_T is the thermal energy of the ions in the liquid, and V is the molar volume. Core brown dwarf temperatures exceed the Debye temperature, and the Dulong and Petit formula for the molar specific heat $C_V = 3R$ is a satisfactory approximation (Debye, 1912). With the pressure in degenerate electrons and the specific heat, entropy, and thermal energy in the ions, the equation of state at high pressures and densities is conceptually clean. However, at pressures at and below P_0, the Coulomb interaction is crucial. A characteristic length, the Bohr radius, appears along with a characteristic density ($\sim$the density of "terrestrial" matter). Since the central pressure of Jupiter (P_{CJ}) is ~ 100 Mbar and $P_{CJ} < P_0$, Coulomb effects make a qualitative difference for objects near Jupiter's mass. For a pure hydrogen plasma, the density-dependent Coulomb correction to the pressure in Eq. (2.21) is a factor of $(1 - 0.85/\rho^{1/3})$, which below $\rho \sim 50$ gm/cm^3 is significant. It is at the onset of Coulomb dominance, with its characteristic density and length scale, that the effective polytropic index slides from $n = 1.5$ through $n = 1.0$ to $n \sim 0.0$ ($\sim$incompressible; see Fig. 1).

At a given density, as the temperature is lowered, Γ increases. According to the classic arguments of Lindemann, the solid$\rightarrow$liquid phase transition occurs when the thermal oscillation of an ion in the harmonic-oscillator potential of its Wigner-Seitz cell achieves some given fraction (ϵ) of r_s ($\epsilon \sim 0.1$, perhaps). Since the mean-squared thermal displacement (ΔX^2) of an ion in a harmonic oscillator is $\sim kT/M\omega^2$, the condition that $(\Delta X/r_s)^2 = \epsilon^2 = (0.1)^2$ translates into a condition on Γ ($< 1/\epsilon^2 \sim 100$). More detailed Monte Carlo calculations (Brush, Sahlin, and Teller, 1966; Slattery, Doolen, and DeWitt, 1982; Stringfellow, DeWitt, and Slattery, 1990) put the transition at $\Gamma = 178$, and this line is shown in Fig. 2. Since none of the brown dwarf trajectories reach this line, we conclude that the solid metallic phase is not of astrophysical importance. In fact, the lightness of the hydrogen nucleus (proton) requires that its zero-point oscillation be included in the Lindemann analysis. When this is naively done, one finds that hydrogen "melts itself" at all temperatures for $\rho > 1$ gm/cm^3 due to its zero-point motion. Indeed, this is what molecular hydrogen does at atmospheric pressure in the laboratory. It is a liquid down to 0 K. However, it has been suggested (Ceperly, 1986; Ceperly and Alder, 1986) that a more rigorous quantum-mechanical calculation allows solid metallic hydrogen/helium mixtures to exist in a restricted region of the ρ-T plane, far below the $\Gamma = 178$ line, at low temperatures ($T < 10^3$ K) and "low" densities ($\rho \leq 10^2$ gm/cm^3). However, in a recent paper, Chabrier, Ashcroft, and DeWitt (1992) argue that the zero-point terms in the solid and liquid phases are comparable and that the critical Γ is little changed. Nevertheless, whether the solid phase obtains is moot for our purposes, as Fig. 2 amply demonstrates.

C. Brown dwarf and M dwarf atmospheres and spectra

As we have shown, the outer radiative skin of a late M dwarf or a brown dwarf is exceedingly thin. With effective temperatures at and below 3500 K, they bear a superficial resemblance to red giants and, by their extreme red colors, could be confused with them. However, the surface gravity of our compact protagonists is some six to seven orders of magnitude larger than that of a giant. Using Eqs. (2.10) and (2.14), we find that the high gravities and the similar or lower effective temperatures imply that brown dwarf and VLM photospheric pressures and densities exceed those of giants by a similar factor. Therefore, the atmosphere, instead of being dominated by atomic species, is composed mostly of molecules. Furthermore, below about 2400 K, grains condense out and can contribute significantly to the continuum opacity. Molecules and grains provide the distinguishing spectral features at the edge of the main sequence. In addition to the molecular hydrogen (H_2) and neutral helium that dominate the atmosphere, H_2^-, H^-, and He^- can be found. The metals are in their neutral, singly and doubly ionized states deep inside the atmosphere at 10^4 K, but near the photosphere are found as hydrides [CaH, MgH, SiH), oxides (TiO, VO), magnesium silicates [e.g., enstatite ($Mg_2Si_2O_6$)], carbides (e.g., Fe_3C), and iron grains. The C/O ratio determines the chemistry of carbon. For C/O > 1, carbon tends to be incorporated in CO and graphite grains, but for C/O < 1 and very low temperatures ($\lesssim 600$ K), it tends to be in CH_4. The abundance of Fe_3C is also regulated by the carbon abundance. Oxygen is not only incorporated in silicates and CO, but in H_2O as well. "Steam" bands play an important role in spectrum formation and may be the most useful brown dwarf signatures, centered as they are near the infrared J, H, and K bands (Berriman and Reid, 1987; Leibert and Probst, 1987; Lunine *et al.*, 1989; Saumon, Lunine, *et al.*, 1992).

With such a plethora of species to consider, the radia-

tive transfer and spectral synthesis calculations are formidable. However, the molecular features in VLM and brown dwarf spectra provide essential and critical diagnostics that must be mastered before cool stars and brown dwarfs are to be understood. The major opacity sources come from H^-, H_2^-, He^-, atomic hydrogen transitions, Rayleigh and electron scattering, bound-free transitions of Mg, Si, and Ca, the electronic bands of MgH, CaH, and SiH, the rotation-vibration transitions of TiO, H_2O, CO, and CN, and the collisionally induced dipole moment of H_2 (Lenzuni, Chernoff, and Salpeter, 1991). The latter is particularly important at low metallicities and in Jupiter's atmosphere. The opacity due to grains requires special knowledge—we need the particle size spectrum ($a \sim 1-10$ μm?), the vertical distribution of the grain "clouds," their patchiness, and their composition. Lunine *et al.* (1989) made the first detailed attempt to understand cloud physics by studying grain coalescence, aggregation, and transport, and the vapor pressure curves of the relevant solids. However, the problem as it stands is too complicated soon to yield, and we must be satisfied at present with low-order approximations and guesses.

Despite these *caveats,* there has been real theoretical progress over the last few years in understanding the emission of cool, dense atmospheres (Lunine *et al.*, 1989; Allard, 1991; Ruan, 1991). Allard's (1991) recent theoretical spectra deserve special mention for their completeness and the clarity with which she has cataloged the spectral systematics with T_e, g, and metallicity. We shall briefly discuss some of her work to provide the reader with a flavor for the theoretical spectra of cool stars. Note, however, that she does not study brown dwarf spectra ($T_e < 2000$ K), but concentrates on late M dwarfs (2000 K $< T_e <$ 3500 K). There are as yet no good theoretical models of brown dwarf spectra (however, see Saumon, Lunine, Hubbard, and Burrows, 1992 and Lunine *et al.*, 1989); so our discussion cannot be as comprehensive as we would like.

Figure 3, taken from Allard (1991), depicts continuum and band opacities (K_λ) versus wave number for $T_e = 3000$ K, $g = 10^5$ cm/s^2, and solar composition at the atmospheric level where τ at the center of the J band ($\lambda = 1.2$ μm) is unity. In the infrared, the rotation-vibration bands of H_2O and bound-free absorption of H_2^-, H^-, and He^- dominate. In the optical, absorption by the molecular bands of TiO and the classic bound-free absorption of H^- dominate. The TiO and VO bands are generally used to determine spectral type for the M dwarfs. However, as T_e decreases, these bands become less and less useful indices of spectral type. Beyond ~M6 a better set of features, perhaps the steam features in the infrared, should be considered to classify the late M dwarfs (Kirkpatrick, Henry, and McCarthy, 1991).

Figure 4 from Allard (1991) shows a synthetic emergent spectrum for $T_e = 3000$ K, $g = 10^5$ cm/s^2, and solar metallicity. The standard photometric filter bands are indicated. The solid line is the complete spectrum, the dotted line is the spectrum with the TiO and H_2O bands and the atomic lines suppressed, and the dashed line depicts a blackbody at 3000 K. Neither M dwarf nor brown dwarf spectra are blackbodies, particularly in the optical where TiO, VO, and the hydrides severely blanket the emission. Most of the energy emerges in the infrared, and there are distinctive H_2O and CO features. The systematic alteration of the M dwarf spectra with T_e from 3250 to 2000 K is depicted in Fig. 5, also from Allard (1991). The dashed lines are the corresponding blackbodies. It can be seen that the H_2O features emerge inexorably with decreasing T_e, and the blackbody approximation completely breaks down. Band absorption causes a systematic shift of the effective peak of the emission to higher frequencies rela-

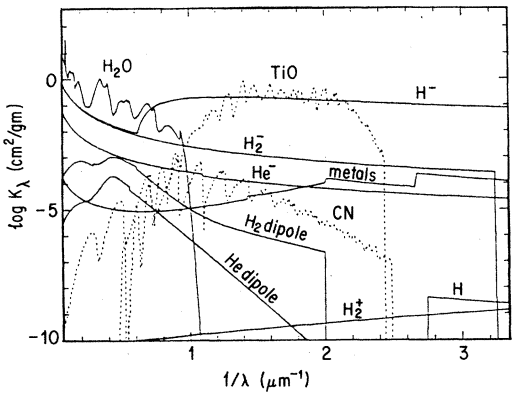

FIG. 3. Opacities (in cm^2/gm) vs wave number (in μm^{-1}) for $g = 10^5$ cm/s^2, solar composition, and $T_e = 3000$ K from Allard (1991). Shown are most of the dominant sources of atmospheric opacity due to H_2O, TiO, H^-, H_2^-, H_2, and metals at a depth such that $\tau(\lambda = 1.2\mu\text{m}) = 1$. Notice the prominent role of H_2O, H^-, and TiO.

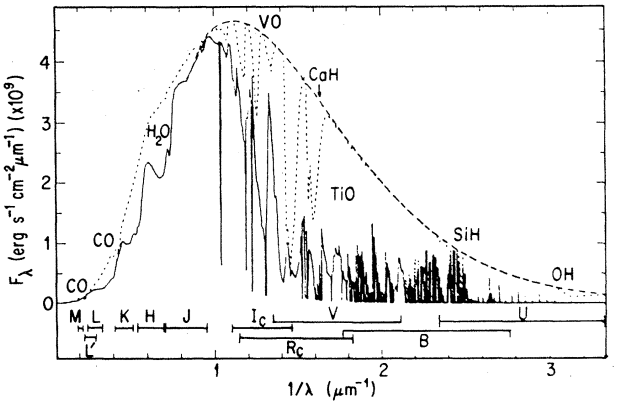

FIG. 4. Complete synthetic emergent spectrum from Allard (1991) for $g = 10^5$ cm/s^2, $T_e = 3000$ K, and solar composition (solid line). The dashed line is a blackbody curve normalized to just envelop the synthetic spectrum, while the dotted line ignores the absorptions due to H_2O, TiO, and metal lines. Notice the distinctive H_2O and CO features in the infrared and the grossly unblackbody behavior in the visible. The regions of the standard photometric bands are superposed for reference.

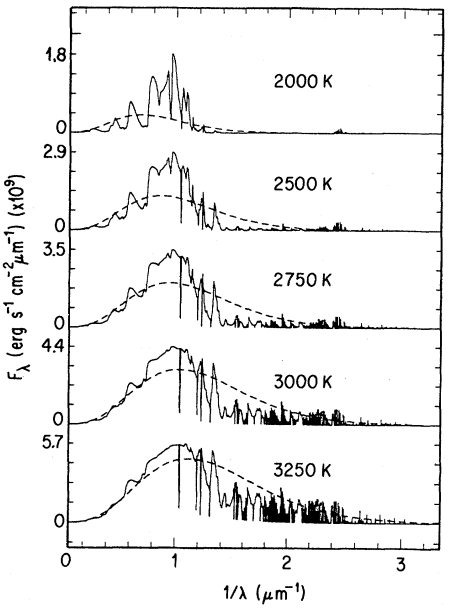

FIG. 5. Same as Fig. 4, but for $T_e = 2000$ K to 3250 K (from Allard, 1991). The dashed curves follow the blackbody function. Theoretical dwarfs are not blackbodies and show a distinctive blueward shift with decreasing T_e from the blackbody. At and below $T_e \sim 2500$ K, the color temperature and T_e can be different by hundreds of K.

tive to the corresponding blackbody peak. This results in a systematic separation of the color temperature and T_e with decreasing T_e, as has been noticed by Berriman and Reid (1987); see also Stringfellow, 1991). Brown dwarfs should continue this trend (Ruan, 1991; Saumon *et al.* 1993).

The Rosseland mean opacities (κ_R) are a bit easier to estimate and generally range between 10^{-3} and 10^{-1} cm^2/gm for solar composition (Tsuji, 1971; Alexander, Johnson, and Rypma, 1983; Lunine, 1986; Lunine *et al.*, 1989; Carson, 1992; Carson, Luo, and Sharp, 1992). It is κ_R that determines the relationship between the central entropy (or the temperature at 10 bars) and T_e and, therefore, the rate at which the thin radiative skin of the brown dwarf releases its bulk internal heat. The atmospheric opacity is the valve that controls the evolutionary history of the brown dwarf.

D. Nuclear rates

As a VLM or brown dwarf contracts early in its evolution due to radiation from its surface, its core temperature increases. This is the classic negative specific-heat effect in stars. The contraction is halted either by the onset of electron degeneracy or by the ignition of thermonuclear fuel, whichever comes first. With degeneracy, since pressure is then only a weak function of temperature or heat content, further photospheric radiation does not lead to significant compression and is accompanied by a decrease in the core temperature. The object then cools "like a rock." If the central temperatures achieved before the onset of degeneracy are sufficient to ignite enough thermonuclear fuel, the object can become a star. If not, it will become a brown dwarf. Only objects with sufficient mass achieve ignition before degeneracy. Hence there is a minimum "stellar" mass (canonically $\sim 0.08 M_\odot$) above which lies the hydrogen main sequence. On the main sequence, photospheric energy losses are balanced by burning in the core.

Since thermonuclear rates are functions of temperature *and* density, the true ignition condition involves both. Hence the ignition temperature is a function of density. Curiously, one finds that at the edge of the main sequence, due to the density increase during final contraction, the core temperature of the transition mass actually begins to decrease before stabilizing at its main-sequence value. Even below the edge of the VLM branch, massive brown dwarfs ($\geq 0.07 M_\odot$) can burn hydrogen for billions of years before their thermonuclear fires are eventually quenched. In fact, down to masses near $\sim 0.015 M_\odot$. (Grossman, 1970; Grossman, Hays, and Graboske, 1974), primordial deuterium is burned during a brown dwarf's first ten million years, and, down to $\sim 0.06 M_\odot$, primordial lithium is consumed, though over a significantly longer time.

The main thermonuclear reactions on the VLM and brown dwarf branches are

$$p + p \rightarrow d + e^+ + \nu_e \quad (Q = 1.442)\,, \tag{2.23}$$

$$p + e^- + p \rightarrow d + \nu_e \quad (pep \text{ process})\,, \tag{2.24}$$

and

$$p + d \rightarrow {}^3\mathrm{He} + \gamma \quad (Q = 5.494 \text{ MeV})\,. \tag{2.25}$$

The core temperatures achieved in these light objects are not sufficient to overcome the Coulomb barriers ($Z = 2$) of the ^{3}He-^{3}He and ^{3}He-^{4}He reactions of the complete *p-p* chain that operates in the sun. Hence the *p-p* chain is truncated and ^{4}He is not produced. The strong-interaction process (2.25) is quick, is the process by which primordial deuterium is consumed, and provides the bulk of the thermonuclear energy. The weak-interaction process (2.23) creates the fresh deuterium and is the rate-limiting link in the burning chain [the *pep* process (2.24) is of secondary importance]. The effective Q value per proton of combined processes (2.23) and (2.25) is $(1.442 - 0.262)/2 + 5.494 = 6.084$ MeV, instead of the 6.901 MeV of the full *p-p* chain. The 0.262 MeV accounts for the average energy of the neutrino (ν_e) lost in process (2.23).

The unscreened energy generation rates of processes (2.23) and (2.25) are (Fowler, Caughlan, and Zimmerman, 1975)

$$\dot{\epsilon}_{pp} = 2.5 \times 10^6 [\rho X^2 / T_6^{2/3}] e^{-33.8/T_6^{1/3}} \ \frac{\text{ergs}}{\text{gm}\,s} \tag{2.26}$$

and

$$\dot{\epsilon}_{pd} = 1.4 \times 10^{24} [\rho X Y_d / T_6^{2/3}] e^{-37.2/T_6^{1/3}} \ \frac{\text{ergs}}{\text{gm s}}\,, \tag{2.27}$$

where Y_d is the deuterium mass fraction whose primordial value is near 2×10^{-5}. (Note that we employ the "dot" to emphasize that this is a rate.) However, since Γ is of order unity, the plasma is strongly coupled, and screening of the protons and deuterons in the above processes can significantly affect the reaction rates. In the intermediate and strong screening limit, the enhancement factor for both processes (2.23) and (2.25) is given by Graboske *et al.* (1973),

$$S \simeq e^{H(0)} , \tag{2.28}$$

where

$$H(0) \simeq \min(0.977\Gamma^{1.29},\ 1.06\Gamma) . \tag{2.29}$$

At the edge of the main sequence, the core S is ~ 2; but lower on the brown dwarf branch, it can be higher.

One can always fit thermonuclear rates to power laws in T and ρ, which obtain over only a narrow range in both, but give a clear indication of the sensitivities. If we set

$$\dot{\epsilon}_n = \dot{\epsilon}_c \left[\frac{T}{T_c}\right]^s \left[\frac{\rho}{\rho_c}\right]^{u-1} , \tag{2.30}$$

we can use (2.26) and (2.28) to derive

$$u = 2 + \frac{1.29}{3} H(0) \tag{2.31}$$

and

$$s = \frac{33.8}{3T_6^{1/3}} - \frac{2}{3} - 1.29H(0) . \tag{2.32}$$

At $T_c = 3\times10^6$ K and $\rho_c = 10^3$ gm/cm^3, conditions characteristic of the core of the transition mass, we derive that $u \sim 2.28$ and $s = 6.31$. These values imply moderately steep dependences and should be compared to $u = 2$ and $s \sim 4$ for the core of the Sun.

E. An analytic model for brown dwarfs

Because brown dwarfs are convective and, hence, isentropic and their equation of state is polytropic both above and below the PPT, all the essentials of brown dwarf cooling theory can be analytically obtained. In this section, we derive $T_e(t,M)$ and $L(t,M)$ using only the scaling laws of a polytrope, the entropy matching condition at the PPT between metallic liquid hydrogen at high densities and molecular hydrogen at low densities, and a crude model of the photosphere. Furthermore, we extend this analysis and derive analytically the value of the minimum hydrogen main-sequence mass. Despite the crudity of the assumptions, the derived power laws are a passable match to the more detailed cooling theory.

When an electron gas is degenerate, the measure of its degeneracy is given by

$$\eta = \frac{\mu_F}{kT} = \frac{(3\pi^2\hbar^3)^{2/3}}{2m_e kT}\left[\frac{\rho N_A}{\mu_e}\right]^{2/3} \tag{2.33}$$

$$= 3.018\times10^5 \left[\frac{\rho}{\mu_e}\right]^{2/3} \Big/ T , \tag{2.34}$$

where μ_F is the electron Fermi energy in the degenerate limit and the other constants have their standard meanings. At high densities and low temperatures (and hence at low entropies), $\eta \gg 1$ and the gas is degenerate, while at high entropies, $\eta \ll 1$ and the ideal-gas law (2.10) obtains. A pressure law that applies at both extremes, but only poorly between them, is

$$P = 10^{13}\left[\frac{\rho}{\mu_e}\right]^{5/3}\left[1+\frac{\alpha}{\eta}\right], \quad \alpha = \frac{5\mu_e}{2\mu} , \tag{2.35}$$

where μ is the mean molecular weight of ionized hydrogen/helium mixtures. For $X = 0.75$ and $Y_\alpha = 0.25$, $\mu_e = 1.143$, $\mu = 0.593$ and $\alpha = 4.82$. The virtue of Eq. (2.35) is its simplicity. (It is not highly accurate for partially degenerate fluids.) The crucial point to notice is that η is approximately constant along adiabats (see Fig. 2). Hence a single value of η is characteristic of the vast bulk of a brown dwarf of a given mass and composition, at a given time. Brown dwarf evolution proceeds from high to low specific entropies ($\sigma = S/kN_A$, where S is the entropy per gram) and from low to high η's. Knowing either $\sigma(t)$ or $\eta(t)$ is equivalent to knowing how brown dwarfs evolve.

Equations (2.2) and (2.35) imply that the polytropic constant is

$$K' = \frac{10^{13}}{\mu_e^{5/3}}\left[1+\frac{\alpha}{\eta}\right] . \tag{2.36}$$

The scaling laws for polytropes [Eqs. (2.6) to (2.8)] and Eq. (2.34) can now be converted into

$$R = 2.3573\frac{K'}{GM^{1/3}}$$

$$= 6.05\times10^9\left[\frac{0.05M_\odot}{M}\right]^{1/3}\left[1+\frac{\alpha}{\eta}\right] \text{ cm} , \tag{2.37}$$

$$\rho_c = 646\left[\frac{M}{0.05M_\odot}\right]^2 \frac{1}{\left[1+\frac{\alpha}{\eta}\right]^3} \text{ gm/cm}^3 , \tag{2.38}$$

$$P_c = 3.67\times10^5\left[\frac{M}{0.05M_\odot}\right]^{10/3} \frac{1}{\left[1+\frac{\alpha}{\eta}\right]^4} \text{ Mbar} , \tag{2.39}$$

and

$$T_c = \frac{3.018\times10^5 \text{ K}}{\eta}\left[\frac{\rho_c}{\mu_e}\right]^{2/3} \tag{2.40}$$

$$= 2.06\times10^7 \text{ K}\left[\frac{M}{0.05M_\odot}\right]^{4/3} \frac{\eta}{(\eta+\alpha)^2} , \tag{2.41}$$

where we have set $\mu_e = 1.143$ for definiteness. When η is finite, the star is thermally expanded; as η increases, the star contracts. The degenerate-star values of P_c, ρ_c, T_c, and R are reached asymptotically as $\eta \rightarrow \infty$.

As is plain from Eq. (2.41), T_c has a maximum for a given mass at $\eta = \alpha$:

$$T_c^{\max} = 10^6 \text{ K} \left[\frac{M}{0.05 M_\odot} \right]^{4/3} . \tag{2.42}$$

Larger masses achieve larger core temperatures. If the mass is sufficient, the core can reach ignition conditions. Equations (2.37)–(2.41) show that when T_c is at peak, $R = 2R(\eta = \infty)$, $\rho_c = \frac{1}{8}\rho_c(\eta = \infty)$, and $P_c = \frac{1}{16}P_c(\eta = \infty)$. Even after $T_c = T_c^{\max}$, the "star" undergoes significant contraction.

The energy equation,

$$\frac{dE}{dt} + P\frac{dV}{dt} = T\frac{dS}{dt} = \dot{\epsilon} - \frac{\partial L}{\partial M} , \tag{2.43}$$

where, again, S is the entropy per mass and the other symbols have their standard meanings, determines the pace of cooling and contraction. Ignoring the energy generation term and integrating over the mass, we find

$$\frac{d\sigma}{dt} \left[\int N_A kT \, dM \right] = -L , \tag{2.44}$$

where L is, of course, the surface luminosity. Solving Eq. (2.34) for T, inserting into the bracketed expression above, and using the polytropic relations $P = K\rho^{5/3}$ and

$$\int P \, dV = \frac{2}{7} \frac{GM^2}{R} , \tag{2.45}$$

we derive

$$\int N_A kT \, dM = 8.93 \times 10^{46} \left[\frac{M}{0.05 M_\odot} \right]^{7/3} \left[\frac{1}{\alpha + \eta} \right] \text{ erg} . \tag{2.46}$$

This is a useful result and is an approximate measure of the thermal energy content of the object. Note the stiff dependence of M. [Curiously, the $\frac{7}{3}$ power appears by analogous arguments in the Thomas-Fermi model of the many-electron atom (Feynman, Metropolis, and Teller, 1949.]

We next turn to an estimate of T_e and L. For this, we employ Eq. (2.14) and the ideal-gas law:

$$P_e = \frac{2}{3} \frac{GM}{R^2 \kappa_R} = \frac{\rho_e N_A k T_e}{\mu} . \tag{2.47}$$

To derive an equation that connects ρ_e and T_e, we avail ourselves of the isentropic condition. Though the atmosphere is by its nature radiative, the entropy at the photosphere is not much different from that in the vast convective regions. Though the entropies are approximately the same exterior and interior to the PPT, the dependences on T and ρ are different—we must match them at the PPT to connect η with T_e. [N.B. However, it may well be a weakly first-order phase transition with $\Delta\sigma \neq 0$ (see Saumon, Hubbard, Chabrier, and Van Horn, 1992).] To do this, we use the approximate analytic expressions for the specific entropy radially above (σ_1) and below (σ_2) the PPT:

$$\sigma_1 = -1.594 \ln\eta + 12.43 \tag{2.48}$$

and

$$\sigma_2 = 1.032 \ln T/\rho^{0.42} - 2.438 , \tag{2.49}$$

where σ_2 is from Stevenson (1991), Y_α has been set equal to 0.25, and σ_1 is a crude fit from the results of Burrows *et al.* (1989). Setting $\sigma_1 = \sigma_2$ (isentropic condition), $T = T_e$, and $\rho = \rho_e$, we obtain

$$T_e = 1.8 \times 10^6 \text{ K} \frac{\rho_e^{0.42}}{\eta^{1.545}} . \tag{2.50}$$

Plugging into Eq. (2.47) and using the polytropic relation

$$g = \frac{GM}{R^2} = 1.8 \times 10^5 \left[\frac{M}{0.05 M_\odot} \right]^{5/3} \frac{1}{(1 + \alpha/\eta)^2} \text{ cm/s}^2 , \tag{2.51}$$

we obtain

$$\rho_e = 1.82 \times 10^{-5} \eta^{1.088} \left[\frac{M}{0.005 M_\odot} \right]^{1.174} \left[\frac{10^{-2}}{\kappa_R} \right]^{0.704} \frac{1}{(1 + \alpha/\eta)^{1.408}} \text{ gm/cm}^3 , \tag{2.52}$$

which when substituted into Eq. (2.50) gives us

$$T_e = \frac{1.84 \times 10^4 \text{ K}}{\eta^{1.088}} \left[\frac{M}{0.05 M_\odot} \right]^{0.493} \left[\frac{10^{-2}}{\kappa_R} \right]^{0.296} \frac{1}{(1 + \alpha/\eta)^{0.59}} . \tag{2.53}$$

We note in passing that Eqs. (2.47) and (2.51) yield

$$P_e = \frac{12.2 \text{ bar}}{(1 + \alpha/\eta)^2} \left[\frac{M}{0.05 M_\odot} \right]^{5/3} \left[\frac{10^{-2}}{\kappa_R} \right] , \tag{2.54}$$

the canonical atmospheric pressure.

Setting $L=4\pi R^2\sigma T_e^4$ (here σ is the Stefan-Boltzmann constant) yields

$$L=1.5L_\odot\left[\frac{M}{0.05M_\odot}\right]^{1.305}\left[\frac{10^{-2}}{\kappa_R}\right]^{1.184}\frac{(1+\alpha/\eta)^{-0.36}}{\eta^{4.352}}\ . \tag{2.55}$$

If we now plug Eqs. (2.46), (2.48), and (2.55) into the energy equation (2.44), we obtain the evolutionary equation for η that we seek:

$$\frac{d\eta}{dt}=2.04\times10^{-14}\left[\frac{0.05M_\odot}{M}\right]^{1.028}\left[\frac{10^{-2}}{\kappa_R}\right]^{1.184}\frac{(1+\alpha/\eta)^{0.64}}{\eta^{2.352}}\ . \tag{2.56}$$

If we ignore the early evolution and assume that $\eta\gg1$, we can drop the $(1+\alpha/\eta)^{0.64}$ term above and integrate. The result is

$$\eta=9.8\left[\frac{t}{10^9\ \mathrm{yr}}\right]^{0.298}\left[\frac{0.05M_\odot}{M}\right]^{0.307}\left[\frac{10^{-2}}{\kappa_R}\right]^{0.353}, \tag{2.57}$$

which, after substituting into Eqs. (2.53) and (2.55), gives us

$$T_e=1551K\left[\frac{10^9\ \mathrm{yr}}{t}\right]^{0.324}\left[\frac{M}{0.05M_\odot}\right]^{0.827}\left[\frac{\kappa_R}{10^{-2}}\right]^{0.088} \tag{2.58}$$

and

$$L=3.82\times10^{-5}L_\odot\left[\frac{10^9\ \mathrm{yr}}{t}\right]^{1.297}\left[\frac{M}{0.05M_\odot}\right]^{2.641}\left[\frac{\kappa_R}{10^{-2}}\right]^{0.35}\ . \tag{2.59}$$

Equations (2.58) and (2.59) encapsulate the analytic theory of brown dwarfs and are surprisingly accurate, given the approximations they embody. (Note that, in the above, we assume that κ_R is independent of time.) It often will prove useful for the reader to refer to these expressions when brown dwarf systematics is discussed, but a few of their noteworthy features bear mentioning here. Foremost is the fact that not only are the powers and trends in Eqs. (2.58) and (2.59) realistic, but the numbers obtained are good to better than 35%, when compared, for example, to detailed model G of BHL, for all but the earliest epochs. The weak dependence on κ_R (especially for T_e) encourages us that this most problematic piece of brown dwarf theory will not, when completely understood, force qualitative changes in our theories. The stiff dependence of L on M reflects the stiff dependence of the binding energy [$\sim GM^2/R\sim M^{7/3}$, cf. Eq. (2.46)] on mass, but is only slightly steeper than the corresponding relation above the transition region on the VLM branch ($L\propto M^{2.2-2.6}$).

The minimum main-sequence mass (MMSM) is derived by setting L_n ($\int\dot\epsilon_n dm$) equal to L [Eq. (2.55)] in Eq. (2.43). If we employ the power-law form [Eq. (2.30)] of $\dot\epsilon_n$, make the polytropic approximation to the structure ($\rho/\rho_c=\theta^n$), and set $T/T_c=(\rho/\rho_c)^{2/3}$ along the core adiabat, we obtain

$$L_n=\int\dot\epsilon_n dm=4\pi a^3\dot\epsilon_c\rho_c\int\theta^b\xi^2 d\xi\ , \tag{2.60}$$

where $b=n(u+\frac{2}{3}s)$. Setting $\theta=1-\xi^2/6\sim e^{-\xi^2/6}$, which is a good approximation in a stellar center (Fowler and Hoyle, 1964), we find

$$L_n=\frac{2.4\dot\epsilon_c M}{(\frac{3}{2}u+s)^{3/2}}=0.079\dot\epsilon_c M\ , \tag{2.61}$$

where $n=1.5$, $u=2.28$ [Eq. (2.31)], and $s=6.31$ [Eq. (2.32)] were used. Plugging Eqs. (2.38) and (2.41) into Eq. (2.60) yields

$$L_n=7.73\times10^4L_\odot\left[\frac{M}{0.1M_\odot}\right]^{11.977}\frac{\eta^{10.15}}{(\eta+\alpha)^{16.466}}\ . \tag{2.62}$$

Equating L_n and L [Eq. (2.55)] gives us

$$2.7\left[\frac{M}{0.1M_\odot}\right]\left[\frac{\kappa_R}{10^{-2}}\right]^{0.111}=\frac{(\eta+\alpha)^{1.509}}{\eta^{1.325}}=I(\eta)\ . \tag{2.63}$$

Equation (2.63) is an implicit equation for $\eta(M)$ along the lower main sequence. The essential fact of Eq. (2.63) is that $I(\eta)$ has a *minimum*. If the mass M is too low, there is no solution to Eq. (2.63). The lowest mass for which there exists a solution to Eq. (2.63) is at the boundary between brown dwarfs and VLM's. The minimum value of the function $I(\eta)$ is 2.337 at $\eta_{\min}=34.7$. Substituting into Eq. (2.63) gives us

$$M=0.0865M_\odot\left[\frac{10^{-2}}{\kappa_R}\right]^{0.111}\frac{I(\eta)}{I(\eta_{\min})}\ , \tag{2.64}$$

and, hence, an MMSM of $0.0865(10^{-2}/\kappa_R)^{0.111}M_\odot$. This number is in excellent agreement with that of the full theory (Kumar, 1963). However, a value of 34.7 for $\eta_{\min}$ is too large. Fortunately, $I(\eta)$ is a very shallow

function of η and, if we put in a more realistic boundary value of η of 9.4, we obtain for the MMSM a value of $\sim 0.1(10^{-2}/\kappa_R)^{0.111} M_\odot$, still respectably close to the actual numerical result. Equation (2.64) also suggests that the dependence of the MMSM on opacity is very weak and inverse. In particular, Eq. (2.64) correctly predicts that the edge mass of the low-metallicity subdwarf population is higher (D'Antona, 1987).

The assumptions concerning the equation of state, the dependences of the nuclear rates, and the constancy of the atmospheric opacities are too crude to allow us to use Eqs. (2.63) and (2.64) to find a reliable $\eta(m)$ relation and, hence, $R(M)$ and $L(M)$ along the lower main sequence. For this, the numerical simulations are required. However, all the systematic behavior of the transition mass and brown dwarf cooling theory are reproduced and summarized by the analytical arguments presented herein.

F. Numerical brown dwarf and M dwarf models

To provide a flavor of the internal structure (and its evolution) of a specific brown dwarf, we display in Sec. II.F.1 thermal and structural profiles for a numerical $0.05 M_\odot$ brown dwarf model at different epochs after formation. Possible cocoon, proto-stellar, T Tauri, and FU Orionis phases that might obtain in the early ($\lesssim 10^6$ yr) stages of a dwarf's life, as well as magnetic activity, rotation, and mass loss, have been ignored. In Sec. II.F.2, we present a complete suite from $0.03 M_\odot$ to $0.2 M_\odot$ of brown dwarf and VLM models and their evolution. For specificity, we focus in both Secs. II.F.1 and II.F.2 on model G of BHL, for which $Y_\alpha = 0.25$ and the mixing length in standard convection theory is one pressure scale height ($\alpha_m = l_p/H = 1$). As was demonstrated in Burrows *et al.* (1989), brown dwarfs are insensitive to α_m, while M dwarf luminosities and effective temperatures show only a weak α_m dependence. The differences between models with $\alpha_m = 1.0$ and the inferred solar value of ~ 1.6 are slight below $0.2 M_\odot$ and we are well within the current model uncertainties. Solar heavy-element abundances were assumed in the opacity calculations.

1. A fiducial $0.05 M_\odot$ brown dwarf model

The evolution of the temperature-density structure of a $0.05 M_\odot$ brown dwarf is depicted in Fig. 6 for times between 5×10^8 and 2×10^{10} yr, inclusive. The profiles at the boundary epochs were reproduced in Fig. 2. The low-density portion of the curve was truncated slightly inward of the photosphere. Notice that T_c can exceed 10^6 K for billions of years and yet not be sufficient to achieve important light-hydrogen fusion rates. During the entire evolution depicted, the entropy per baryon per Boltzmann's constant (σ) decreases a paltry 2 units from ~ 9.0 to 7.0. The first few million years (not depicted) involved the largest entropy changes and witnesses the destruction of primordial deuterium (Stringfellow, 1991). All brown dwarfs more massive than $\sim 0.015 M_\odot$ consume deuterium during this early epoch.

Figure 7 shows the temperature profile for the baseline $0.05 M_\odot$ brown dwarf. The shallow T-versus-M (enclosed mass) curve and its steady decay are in evidence. Perhaps more interesting is the density profile and its evolution during the same epochs (Fig. 8). The model evolves monotonically from the lower curve to the higher solid curve. At 2×10^{10} yr, ρ_c is 651 gm/cm^3, and almost the entire object is found at densities far in excess of the ~ 1.0 gm/cm^3 of the PPT. Closer inspection of Fig. 8 reveals that the density profile maintains its self-similar, polytropic ($n \sim 1.5$) behavior from epoch to epoch.

The radius versus interior mass at the two boundary epochs of 5×10^8 and 2×10^{10} yr is shown in Fig. 9. No-

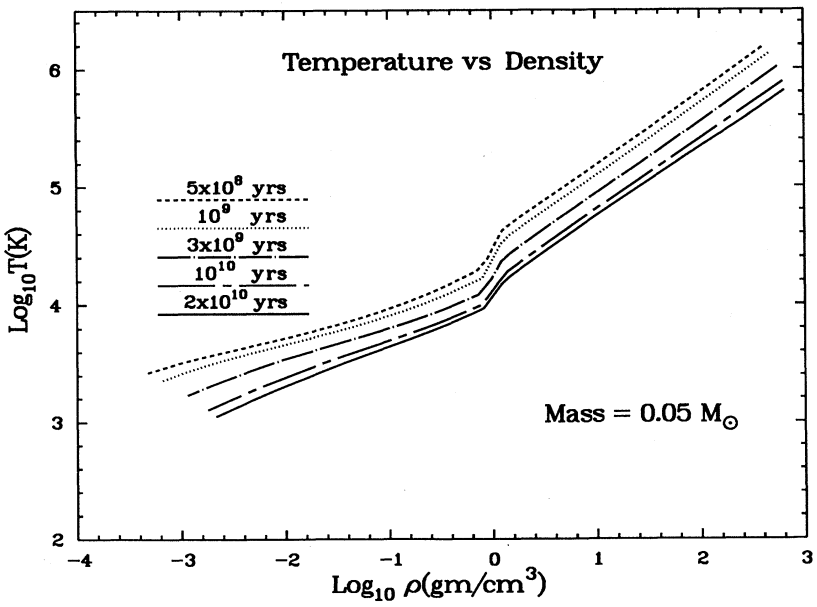

FIG. 6. Profiles of temperature (in K) vs density (in gm/cm^3) for a theoretical $0.05 M_\odot$ brown dwarf at various times after formation. These lines are adiabats. Model G (BHL) parameters were employed. See text for discussion.

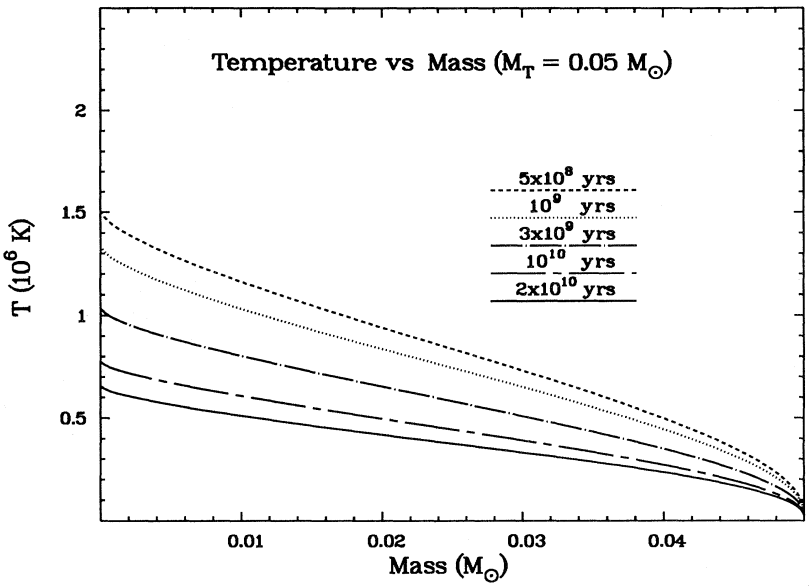

FIG. 7. Temperature (in K) vs enclosed mass (in $M_\odot$) at various times for a model G $0.05M_\odot$ brown dwarf. See BHL and the text for a more complete discussion.

tice that the half-radius point roughly coincides with the half-mass point and that Fig. 8 can be derived from Fig. 9 by using the relation $\rho=[4\pi r^2 dr/dM]^{-1}$. Finally, the pressure profiles at the two boundary times are depicted in Fig. 10. Plotted is the pressure versus the fractional *exterior* mass. The stellar center (on the left) is at $\Delta M=M_T$ and the periphery is beyond the right at $\Delta M \ll M_T$. This figure serves to demonstrate the extremes of pressure encountered in the object. The pressure at the atmosphere ($\sim 10^{-5}$ Mbar) is not even shown on the graph, yet it depicts a run of eight orders of magnitude from a core value in excess of 10^5 Mbar [see Eq. (2.39)]

Figures 6–10 as a set summarize the interior structure of a representative brown dwarf at $0.05M_\odot$ and its evolution.

2. Theoretical brown dwarf and M dwarf properties and evolution: $0.03M_\odot$–$0.2M_\odot$

Here we present with graphs and a table the results of numerical simulations for model G of BHL both above and below the main-sequence transition mass. The purpose of this subsection is to provide benchmark numbers for theoretical brown dwarf and VLM models. Table I shows T_e, L, R, T_c, ρ_c, σ, and L_n/L (the ratio of the total nuclear energy generated to the photospheric luminosity) for various masses between $0.03M_\odot$ and $0.2M_\odot$, at various times. If the latter (L_n/L) is 1, the object has arrived on the main sequence. The MMSM for these models was $0.0775M_\odot$. Notice that $L\sim 10^{-4}L_\odot$, $T_e\sim 1800$ K, $R\sim 6\times 10^9$ cm, and $T_c\sim 2.7\times 10^6$ K at the edge of the main sequence. These values depend on the

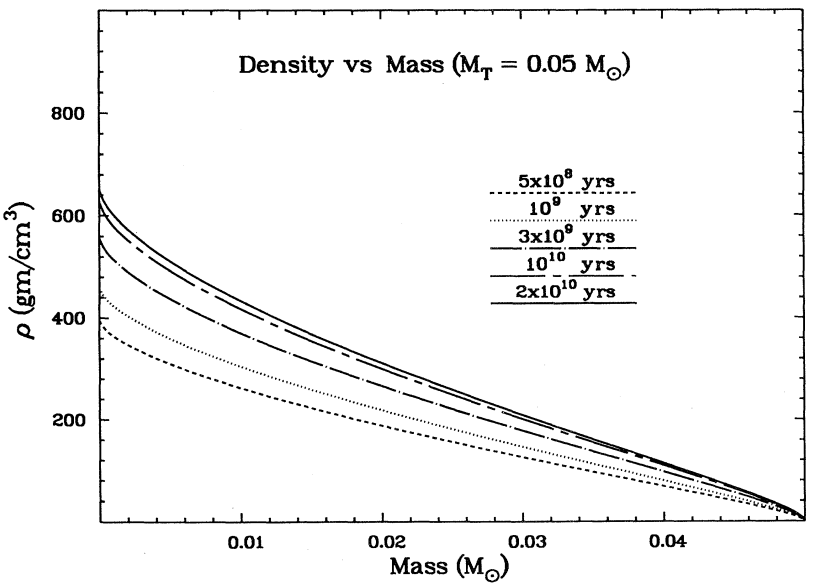

FIG. 8. Same as Fig. 7, but for density (in gm/cm^3) vs enclosed mass (in $M_\odot$). The depicted structure is almost polytropic ($n=1.5$) and the evolution depicts self-similar contraction. Note that at and after 2×10^{10} yr, the structure is no longer changing.

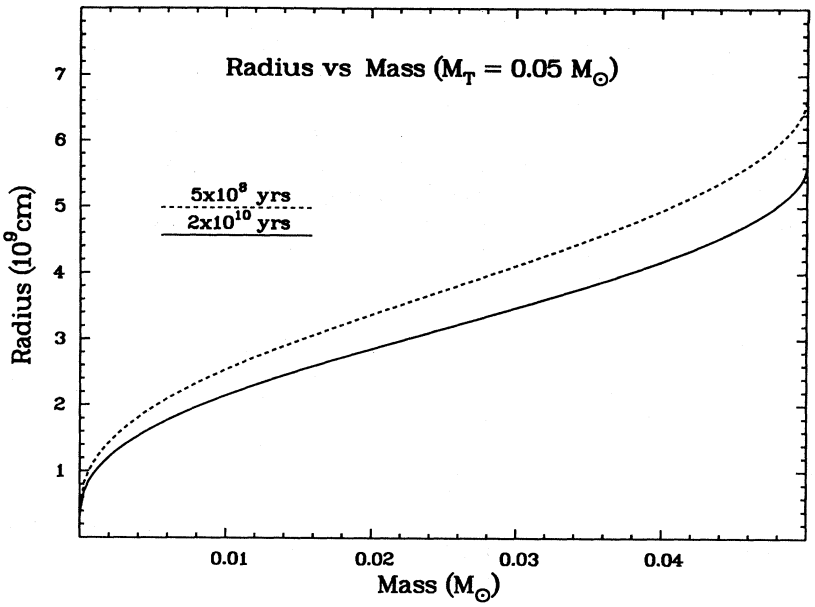

FIG. 9. Same as Fig. 7, but for radius (in 10^9 cm) vs enclosed mass (in $M_\odot$). Only curves for $t=5\times10^8$ and $t=2\times10^{10}$ yr are shown.

opacities, metallicities, Y_α, and the mixing-length parameter in various ways and are particularly sensitive to Y_α near the MMSM. For instance, L varies at $0.08M_\odot$ by a factor of 5 as Y_α changes from 0.22 to 0.28. However, since the actual value of the MMSM moves down as Y_α moves up (MMSM$=0.075M_\odot$ at $Y_\alpha=0.28$), the value of L at the rolling MMSM is not as highly variable. The stiff dependence on Y_α of T_e near the transition mass is depicted in Fig. 11. Though for model B $Y_\alpha=0.22$ and for model I $Y_\alpha=0.28$, they are similar to model G in all other ways. These isochrones at 10^8, 10^9, and 10^{10} years show that though the Y_α dependence is weak at early times, at higher mass, and at lower mass, near the transition mass at 10^{10} years T_e can vary by 1000 K.

Figure 12 depicts T_c versus time for various masses above and below the VLM/brown dwarf boundary. For all masses, the peak central temperature is reached within a few hundred million years, but only for the more massive objects does T_c eventually stabilize at a main-sequence value. At later times, the VLM and brown dwarf branches bifurcate, though just below the edge of the main sequence thermonuclear burning can proceed for billions of years. (N.B. The behavior at $M=0.075M_\odot$.) Notice that for $M\sim0.08M_\odot$, the main-sequence T_c is lower than its peak value. Though T_c decreases for a billion years, the increase in ρ_c more than compensates in the nuclear rate to lift the star onto the main sequence. Figure 13 recapitulates the behavior

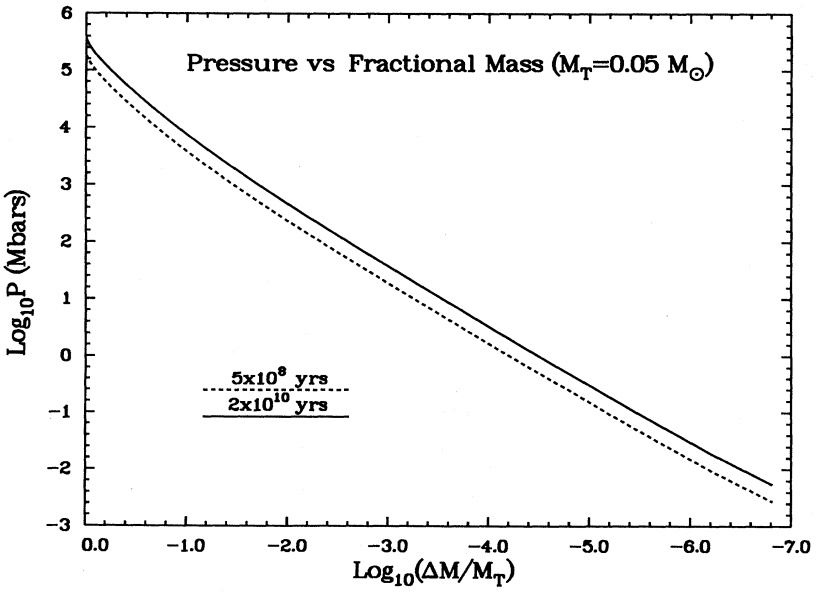

FIG. 10. Same as Fig. 7, but for pressure (in Mbar) vs fractional *exterior* mass ($\Delta M/M_T$), at $t=5\times10^8$ and 2×10^{10} yr. The center is at the left and the PPT is near $\Delta M/M_T\sim10^{-4}$. See the text for a cursory discussion.

shown in Fig. 12 for the same object masses. Though L_n/L can reach 80% and stay above 50% for many billions of years, objects just below the MMSM will eventually fade into oblivion. Even if a star reaches the main sequence, it may take billions of years to do so. These shared properties of "stars" just above and below the transition mass serve to punctuate the fact that what is, or is going to be, a star can be observationally ambiguous and that there is a transition *region* between the VLM and brown dwarf branches. However, after VLM's reach the main sequence they can burn quietly for 10^{11-12}yr, far longer than a Hubble time.

Figure 14 depicts the luminosity (L) and bolometric magnitude (M_B) versus mass at 10^8, 3×10^8, 10^9, 3×10^9, and 10^{10} years. Superposed are data from Liebert and Probst (1987) and McCarthy *et al.* (1988). The approximately power-law cooling behavior of brown dwarfs derived in Sec. II.E is manifest, as is the steep dependence

TABLE I. Model G ($0.03M_\odot < M < 0.2M_\odot$).

Mass ($M_\odot$)	Time (Gyr)	T_e (K)	L ($L_\odot$)	R (Gcm)	T_c ($\times10^6$)	ρ_c (gm/cm^3)	σ	L_n/L
0.200	10.000	3500.0	0.666E−02	15.40	6.140	144.0	13.07	1.000
0.150	10.000	3340.0	0.358E−02	12.40	5.420	206.0	12.22	1.000
0.125	0.100	3260.0	0.302E−02	12.00	4.580	188.0	11.96	0.323
	1.000	3230.0	0.230E−02	10.70	4.950	267.0	11.61	0.997
	10.000	3230.0	0.230E−02	10.70	4.950	267.0	11.61	1.000
0.110	0.100	3200.0	0.253E−02	11.40	4.130	190.0	11.71	0.178
	1.000	3150.0	0.164E−02	9.47	4.590	332.0	11.12	0.990
	10.000	3150.0	0.164E−02	9.45	4.590	334.0	11.12	1.000
0.100	0.100	3160.0	0.224E−02	11.00	3.810	191.0	11.52	0.109
	1.000	3060.0	0.120E−02	8.59	4.270	401.0	10.70	0.982
	10.000	3060.0	0.120E−02	8.57	4.280	404.0	10.69	1.000
0.095	0.100	3130.0	0.209E−02	10.80	3.640	192.0	11.41	0.083
	1.000	2980.0	0.971E−03	8.14	4.070	447.0	10.45	0.968
	10.000	2970.0	0.957E−03	8.10	4.080	453.0	10.43	1.000
0.090	0.100	3110.0	0.194E−02	10.60	3.470	192.0	11.30	0.061
	1.000	2870.0	0.740E−03	7.63	3.820	510.0	10.15	0.938
	10.000	2860.0	0.714E−03	7.56	3.820	525.0	10.11	1.000
0.085	0.100	3080.0	0.179E−02	10.40	3.290	193.0	11.18	0.044
	1.000	2720.0	0.513E−03	7.09	3.490	597.0	9.77	0.858
	10.000	2670.0	0.447E−03	6.88	3.440	653.0	9.63	0.997
	20.000	2670.0	0.446E−03	6.88	3.440	654.0	9.63	1.000
0.080	0.100	3050.0	0.164E−02	10.10	3.110	193.0	11.05	0.031
	1.000	2500.0	0.318E−03	6.59	3.050	697.0	9.33	0.650
	10.000	2100.0	0.134E−03	6.05	2.730	894.0	9.85	0.997
	20.000	2100.0	0.133E−03	6.05	2.720	895.0	8.85	1.000
0.075	0.100	3010.0	0.149E−02	9.98	2.930	194.0	10.91	0.021
	1.000	2200.0	0.173E−03	6.28	2.610	748.0	8.97	0.418
	10.000	1460.0	0.264E−04	5.62	1.990	1040.0	8.17	0.650
	20.000	1080.0	0.721E−05	5.32	1.540	1220.0	7.62	0.447
0.070	0.100	2960.0	0.132E−02	9.65	2.730	194.0	10.76	0.013
	1.000	1890.0	0.910E−04	6.19	2.270	723.0	8.77	0.267
	10.000	988.0	0.514E−05	5.38	1.350	1090.0	7.53	0.181
	20.000	715.0	0.135E−05	5.27	1.110	1160.0	7.23	0.155
0.060	0.100	2820.0	0.983E−03	9.16	2.320	191.0	10.43	0.005
	1.000	1590.0	0.460E−04	6.24	1.760	597.0	8.55	0.053
	10.000	761.0	0.190E−05	5.51	1.010	859.0	7.33	0.024
	20.000	584.0	0.639E−06	5.43	0.834	895.0	7.09	0.015
0.050	0.100	2630.0	0.678E−03	8.70	1.870	183.0	10.05	0.001
	1.000	1400.0	0.290E−04	6.37	1.340	458.0	8.37	0.005
	10.000	645.0	0.105E−05	5.72	0.775	627.0	7.24	0.002
	20.000	508.0	0.394E−06	5.64	0.655	651.0	7.02	0.001
0.040	0.100	2340.0	0.379E−03	8.26	1.390	166.0	9.59	0.000
	1.000	1210.0	0.169E−04	6.56	0.963	328.0	8.18	0.000
	10.000	548.0	0.600E−06	5.98	0.572	428.0	7.15	0.000
	20.000	436.0	0.236E−06	5.91	0.493	443.0	6.93	0.000
0.030	0.100	1850.0	0.143E−03	8.12	0.940	127.0	9.18	0.000
	1.000	975.0	0.781E−05	6.82	0.645	211.0	7.97	0.000
	10.000	452.0	0.309E−06	6.31	0.389	263.0	7.05	0.000
	20.000	364.0	0.127E−06	6.23	0.344	272.0	6.82	0.000

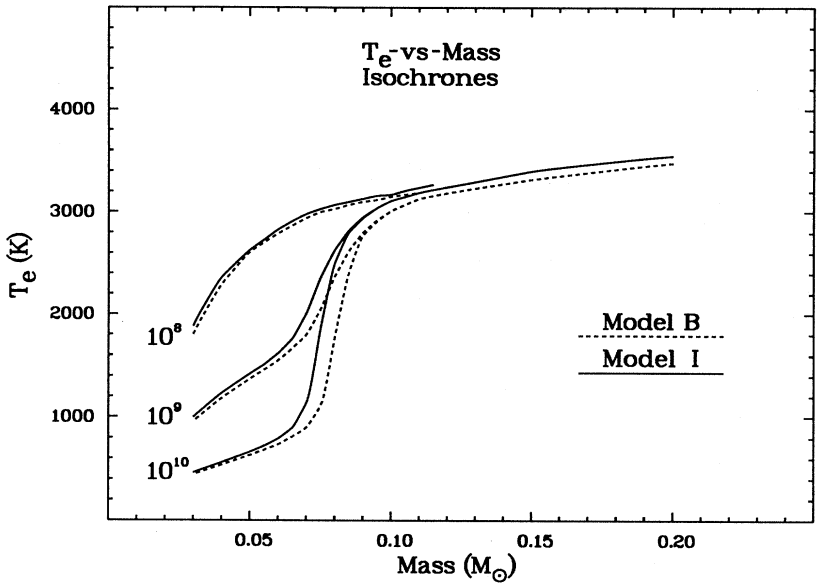

FIG. 11. T_e-vs-M isochrones at $t=10^8$, 10^9, and 10^{10} yr for models B and I. These models are the same as model G (see text), but have helium fractions (Y_α) of 0.22 and 0.28, respectively. Note the sharp dependence on Y_α near the transition zone.

at late times of L on M near $0.08M_\odot$. In this transition region, at 10^{10} years $L \propto M^{20}$, though $L \propto M^{2.2-2.6}$ just above $0.1M_\odot$ and $L \propto M^{2.5-3.0}$ just below $0.06M_\odot$. Figure 15 shows the corresponding T_e-versus-mass isochrones. Notice that brown dwarfs with masses near or below $0.03M_\odot$ cool below 1000 K within only 10^9 years and that *young* brown dwarfs can be mistaken for stars if their ages are not known. This age ambiguity is one of the central problems in distinguishing brown dwarfs from VLM's (see Sec. III). Complicating the identification of brown dwarfs is a pronounced selection bias for luminous objects. These *caveats* alone demand caution when touting putative substellar objects.

Figure 16 compares the radius-versus-mass plot for model G at 10^8 and 10^{10} yr with those for various other models (B, C, D, E) from Burrows, Hubbard, and Lunine (1989) (BHL) (at 10^{10} yr) and the radius-mass curves of various other theorists (Grossman, Hayes, and Graboske, 1974, G74; Vandenberg *et al.*, 1983, V83; Rappaport and Joss, 1984, RJ84; D'Antona and Mazzitelli, 1985, DM85). Model B has a Y_α of 0.22; models C and D have mixing-length parameters of 0.5 and 0.1, respectively, and a Y_α of 0.22; and model E, also with a Y_α of 0.22, has a low opacity as well. All the other properties of these models are the same as in model G. Figure 16 shows that despite the manifold differences between the models displayed, theorists believe that the radii can be accurately predicted. The characteristic $n=1.5$ depen-

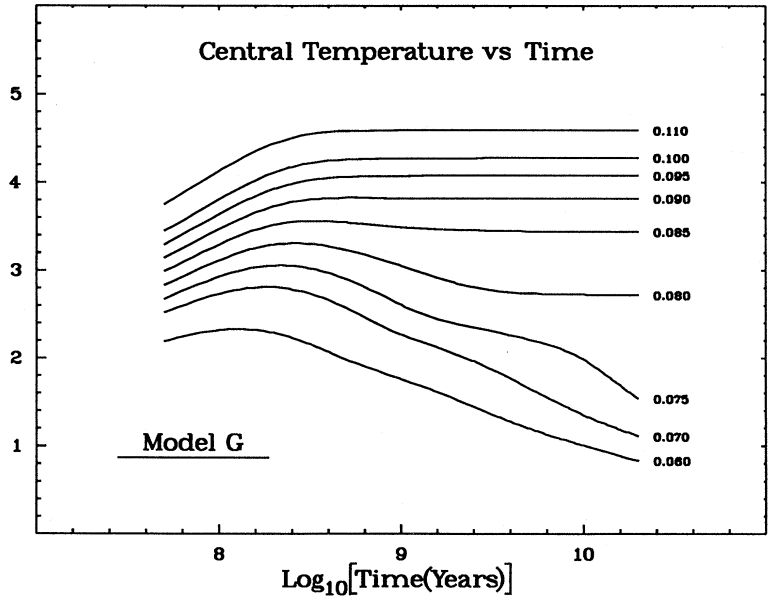

FIG. 12. Central temperature (T_c) vs time (in years) for models with masses between $0.06M_\odot$ and $0.11M_\odot$. There is a clear bifurcation between brown dwarfs and VLM's, though the $0.075M_\odot$ model is hung up by thermonuclear burning for billions of years. Notice that the peak central temperature is reached within only a few hundred million years for all masses, but that it can then decrease before stabilizing even for main-sequence stars.

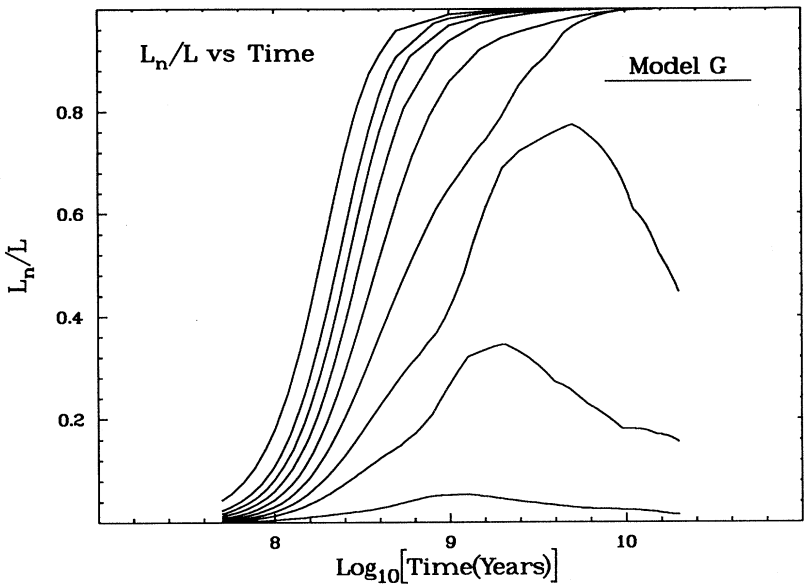

FIG. 13. Similar to Fig. 12, and for the same masses in the same order, but L_n/L vs time (in years). L_n/L is 1 for a star on the main sequence. Notice how large this ratio can be for an object just below the main-sequence transition mass.

dence of R versus $M(R \sim M^{-1/3})$ is clear on the brown dwarf branch, as is the $R \propto M^{0.8}$ behavior on the VLM branch. Notice that there is a minimum radius, depending most sensitively on Y_α and the opacity, that hovers near 5×10^9 cm ($\sim 7\%$ of $R_\odot$).

The evolution of the central density (ρ_c) with time for various masses is depicted in Fig. 17. These curves show how much ρ_c can change in the transition region, even after 10^8 yr. A peak ρ_c of ~ 1200 gm/cm^3 can be reached by brown dwarfs just below the MMSM and, at late times, ρ_c drops precipitously on either side of this peak. The brown dwarf side of the late isochrone roughly reproduces the $\rho_c \propto M^2$ behavior of an $n=1.5$ polytrope. Figure 18, which depicts the surface gravity g versus mass versus time, looks somewhat similar to Fig. 17, but involves what is, in principle, an observable. Either by a measure of both M and R, or by extraction via detailed spectral analysis (Ruan, 1991), g is one of the testable quantities of the theory. Notice that g generally stays below 3.5×10^5 cm/s^2 and does not flirt with 10^6 cm/s^2.

Figures 11–18, and Table I summarize the numerical theory of brown dwarfs, VLM's, and the main-sequence transition zone. To them should one liberally refer for the generic characteristics of these objects.

III. SEARCHES FOR BROWN DWARFS

As demonstrated in Sec. II, the theory of brown dwarfs and the edge of the hydrogen main sequence is well developed and mature. However, the translation between the theorist's vocabulary and that of the observer is made awkward by the continuing lack of good theoretical spec-

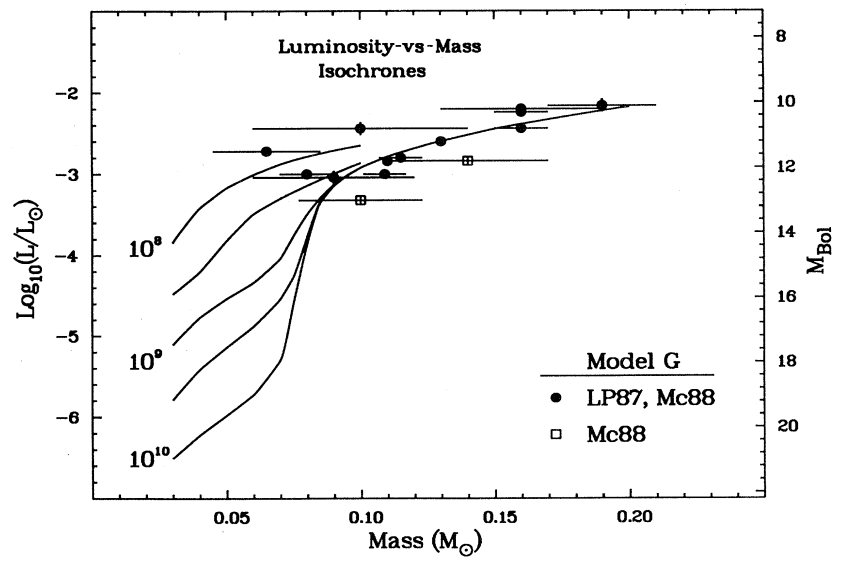

FIG. 14. Photospheric luminosity (L, in units of $L_\odot$) and bolometric magnitude (M_B) vs mass from $0.03M_\odot$ to $0.2M_\odot$ at 10^8, 3×10^8, 10^9, 3×10^9, and 10^{10} years. Model G parameters are employed. Data from Liebert and Probst (1987; LP87) and McCarthy *et al.* (1988; Mc88) are superposed with error bars. The brown dwarf branch is to the left and the VLM branch is to the right.

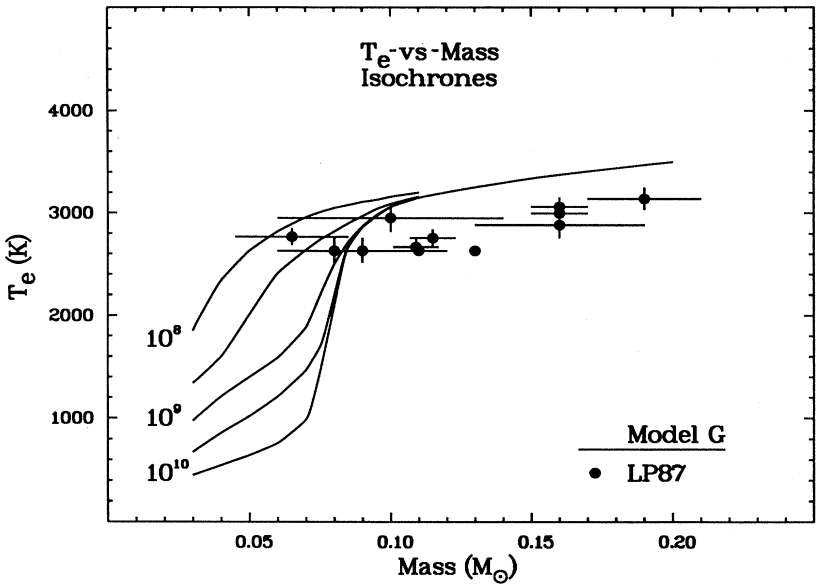

FIG. 15. Same as Fig. 14, but for T_e (in K) vs mass. Only the data from Liebert and Probst (1987) are included.

tra below 2500 K. Most of the data involve photometry and, hence, colors and magnitudes, while theorists still work with T_e and bolometric luminosity. In this section, we employ the observer's vocabulary, not emphasizing the physics of the model interiors, but the observables and the astronomical techniques employed to study dim stellar objects.

We divide the searches to discover substellar objects and to assess their space density into searches for single objects of the heterogeneous galactic disk population (Sec. III.A), searches restricted to a young cluster or star-forming clouds (Sec. III.B), searches for binary companions (which might at times be called planets; Sec. III.C), searches for halo brown dwarfs (Sec. III.D), and searches via gravitational microlensing (Sec. III.E). The searches are further subidivided according to the survey technique used.

A. Searches for single objects

1. Faint stellar objects: Low-mass stars or brown dwarfs?

Isolated stellar objects in the field present the greatest problem in answering the question of whether they are stellar or substellar. There is no direct way to measure the critical parameter—the mass—and their ages may be estimated only crudely based on the space motions, rotation rate, and/or the strength or absence of surface activity. The only way to distinguish an isolated substellar object from a low-luminosity star, at present, is to derive precise estimates of the effective temperature and the luminosity, and to try to match this position in what astronomers call the Hertzsprung-Russell (HR) diagram with an evolutionary track of unique mass and age.

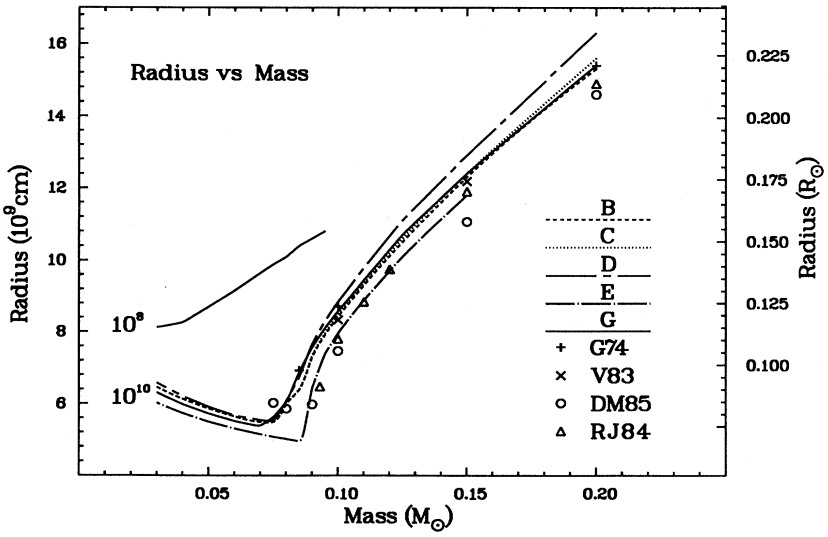

FIG. 16. Radius (in 10^9 cm and $R_\odot$) vs mass (in $M_\odot$) at 10^8 yr (for model G) and 10^{10} yr (for models G, B, C, D, E and from the calculations of other theorists). G74 is Grossman *et al.* (1974), V83 is Vandenberg *et al.* (1983), DM85 is D'Antona and Mazzitelli (1985), and RJ84 is Rappaport and Joss (1984). Models B–E are described in Burrows *et al.* (1989) and in the text. Radii in the cold brown dwarf region (bottom left) are generally around $0.1R_\odot$. The VLM branch is to the right.

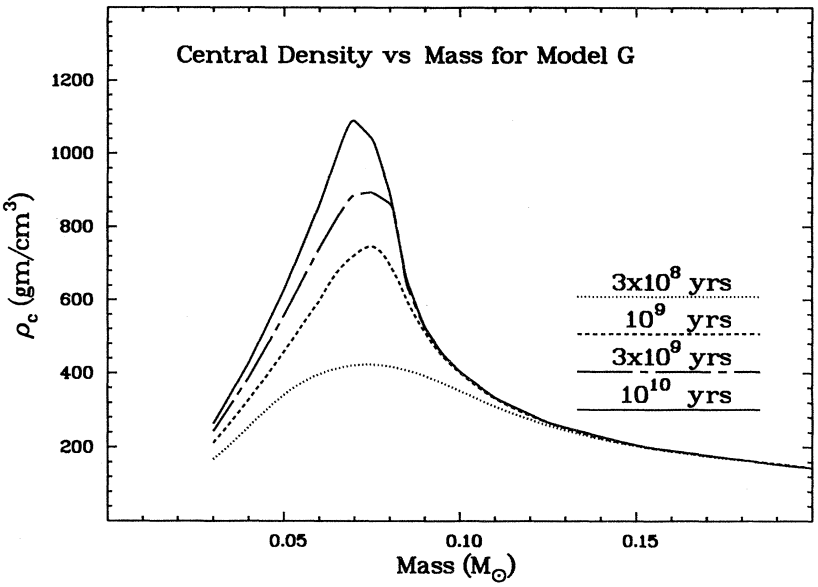

FIG. 17. Evolution of the central density [ρ_c (in gm/cm^3)] with time along the brown dwarf/VLM mass continuum. Brown dwarfs occupy the left and peak regions and VLM's occupy the right. Notice that ρ_c's above 10^3 gm/cm^3 can be achieved in the transition region.

The quandary faced in trying to do this fit is immediately apparent in Fig. 19, adapted from Liebert (1991). The slopes of the locus of points for low-mass stars (called the zero-age main sequence or ZAMS) and the substellar evolutionary tracks are quite similar, with the positions of the latter only 100–300 degrees cooler at a given luminosity. Note that the former remain essentially unevolved in position for tens of gigayears until hydrogen is completely exhausted in a completely convective star.

Shown also are some of the faintest known stellar objects, plotted with best estimates of these parameters. Given the impossibility of determining T_e to better than a few hundred degrees, it is possible, by moving the data points to modestly higher T_e, to fit these data points as VLM stars of moderate to old age. If the points fall to the right of the ZAMS locus, they may fit the contracting tracks of young, substellar objects. The lower the T_e value one assumes at a given L, the lower is the mass and the younger the age.

Hence T_e is a critical parameter when the age and mass are otherwise unknown, yet it is not accurately determined by the comparison of current observations with current atmospheric and interior models. All values of T_e, until very recently, were based on fits of observed spectral energy distributions or colors to *blackbodies,* not to synthetic spectra predicted from realistic model atmospheres. As we implied in Sec. II.C, the Ph.D. dissertations of Allard (1991) and Ruan (1991) represent the first attempts to apply model atmospheres to some observations of very-low-luminosity objects. However, only partial success has been achieved. Ruan (1991) concludes

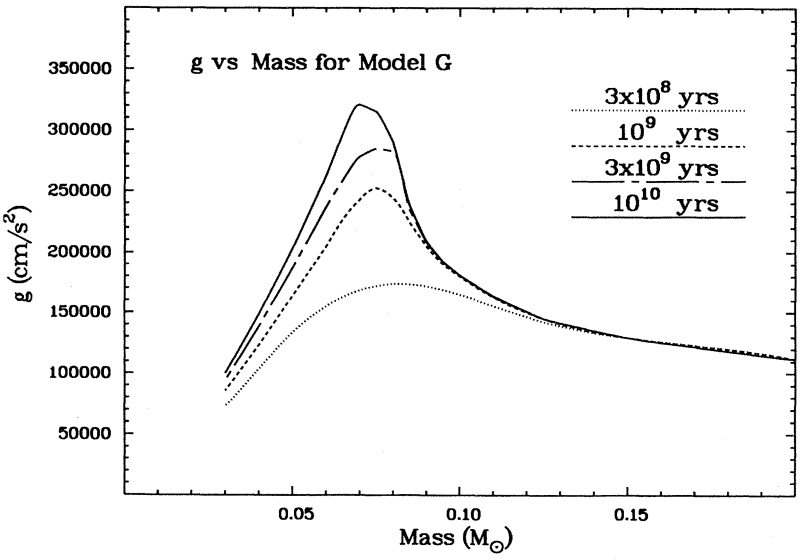

FIG. 18. Same as Fig. 17, but for surface gravity (g, in cm/s^2) vs mass (in $M_\odot$) at various times between 3×10^8 and 10^{10} years, inclusive. See text for a brief discussion.

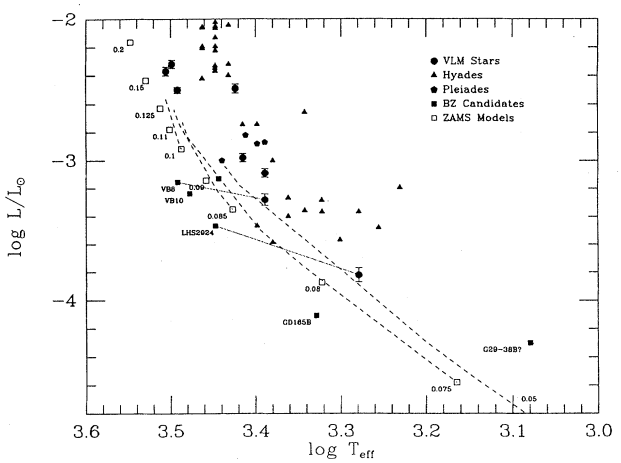

FIG. 19. Adapted from Liebert (1991), some recent attempts to place VLM stars and brown candidates onto a true HR diagram. Solid circles are VLM stars observed and analyzed by Berriman and Reid (1987). Pleiades candidates from Stauffer *et al.* (1989) are also plotted. Benchmark stars vB8, vB10, and LHS2924 are plotted twice as solid circles (Berriman and Reid estimates) and solid squares (Becklin and Zuckerman, 1988, estimates), illustrating the range of recent temperature determinations at the lowest luminosities. Included also are the resolved Becklin and Zuckerman source GD165B, and the unresolved G29-38B(?), assuming the infrared excess of the latter is attributable to a companion. The open squares are hydrogen-burning model positions for an age of 10^9 years, with prior evolutionary tracks (shown as dashed lines) at $0.1M_\odot$ and below. Shown, too, is a brown dwarf track for $0.05M_\odot$ with no terminus (rightmost dashed line).

from the difficulty in fitting observations that the atmospheric stratifications of her models may be incorrect; certainly this implies that the T_e determinations remain less accurate than the key value of a few hundred degrees required for Fig. 19. Finally, even if one could place the stars perfectly in T_e and L, there remain uncertainties associated with the interior models which affect the predicted positions of tracks in the HR diagram, just as they do the other parameters plotted in Figs. 6–18.

At face value, in Fig. 19 the "best" current estimates of T_e and L for the lowest-luminosity known stellar objects would imply that most of these are brown dwarfs. Given the expectation that most stars in the galactic disk are old rather than young (i.e., less than 1 Gyr or so), one may argue that the bulk of the points should fit the low end of the ZAMS instead. This would imply either that the empirical fits are yielding values of T_e that are too low, and/or that the theoretical tracks predict ZAMS temperatures that are too high. The latter possibility may imply that the radii of the interior models are too small, even though one might surmise from Sec. II.F.2 and Fig. 16 that the radii are the best theoretically predicted quantities.

2. Construction of initial mass functions for field stars

The function that describes the number of stars in each interval of luminosity for a stellar population is called the luminosity function (LF). For the main sequence, the luminosity of a star is normally a power-law function of the mass, over a limited interval of mass:

$$L \propto M^a , \tag{3.1}$$

where a is generally found to vary from 3 to 5 over the stellar mass range above $0.3M_\odot$. The a index varies from 2.2 to 2.6 between 0.1 and $0.3M_\odot$. Thus, if we want to determine the initial mass function (IMF) for low mass and VLM stars whose present-day luminosities are close to their luminosities when they first reached the main sequence, the simplest procedure (and that used most often) is to use the above *M-L* relation with the appropriate exponent to convert an entire LF into the IMF.

The appropriate version of Eq. (3.1) can be determined from a sequence of stellar interior models having different masses, if a uniform chemical composition for the population can be assumed (see Sec. II). The nearby stars of the galactic disk population—certainly an important sample—will be an unknown mix of metallicities. It should be noted that work on M dwarf atmospheres (see especially Ruan, 1991) has progressed to the point where only rudimentary atmospheric abundance estimates for individual stars can be achieved, perhaps to within factors of 2 to 3. However, one can also estimate the *M-L* relation empirically using stellar components in noninteracting binary systems where the masses have been determined by solving the orbits. Figure 20 is a plot of stars with such determinations from Henry (1991). The correlation coefficient for the power-law fit indicates that a simple, linear relation in a log-log diagram,

$$\log(M/M_\odot) = -0.166M_K + 0.560 , \tag{3.2}$$

is a good approximation over the range $0.1-1M_\odot$.

Application of either theoretical models or an empirical *M-L* relation becomes much more complicated as the limiting mass near $0.075-0.08M_\odot$ is approached. This is seen by examination of a similar *M-L* plot of the region of stars of lowest mass, as shown in Fig. 21, also from Henry 1991; see Secs. II.F and III.C.4). In Fig. 21, the absolute 2.2 micron K magnitude is used in place of $\log L$, since it is a directly measurable quantity closely related to $\log L$. Data points are again VLM stars with astrometric mass determinations, with large horizontal error bars, and almost negligible vertical error bars; both the trignonometric parallaxes and the apparent K magnitudes of these nearby stars are accurately measurable. Shown also in Fig. 21 are two sets of theoretical tracks showing the luminosities of stars at a given mass and age, from D'Antona and Mazzitelli [1985 (DM)] and Burrows *et al.* (1989). At a given mass, the models predict a spread of only about one magnitude in luminosity for ages of 0.1–10 Gyr and masses $\geq 0.12M_\odot$. Below this value, the model luminosities diverge rapidly as the mass limit is approached. However, the small number of relevant data points do not show this effect.

The luminosity-mass transformation can be done in two ways. Since the observed *M-L* line does not appear

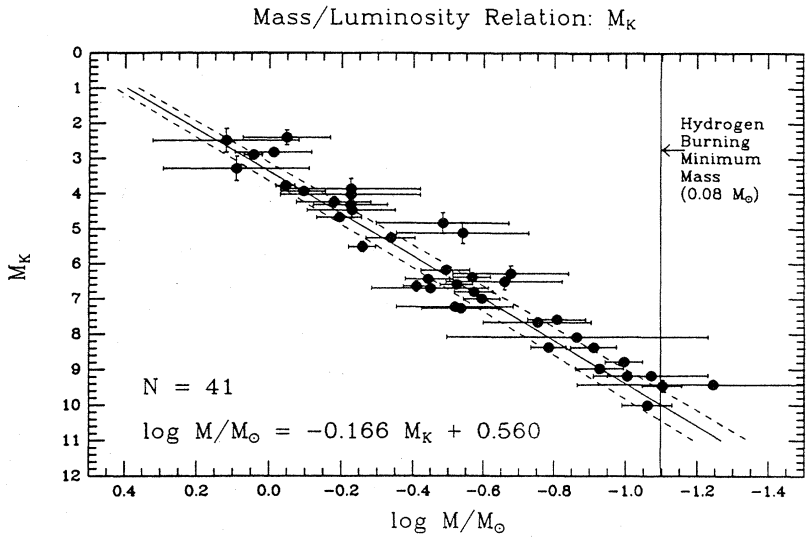

FIG. 20. Mass-luminosity relation at K. The solid line is the weighted linear least-squares fit to the data. The dashed lines represent the fits with 1σ errors in the slope and intercept adopted. Taken from Henry (1991).

to deviate from the general fit near the stellar mass limit, a purely empirical method would be to use Eq. (3.2) as the ordinate in order to transform the luminosity of a single object in the sample into a mass. This approach is widely used in the literature, as we shall show in the following sections. Assuming that the empirical line corresponds with theoretical model lines is equivalent to assuming that the stars of lowest luminosity are mostly younger than 1 Gyr, since the empirical line lies above and to the right of the 1 Gyr tracks. It is implausible to assume that the majority of M stars in the solar neighborhood are younger than 1 Gyr, *unless perhaps they are mostly brown dwarfs.* If, instead, the VLM star formation rate has been constant to within factors of 2 or 3 for the history of the galactic disk, then the mean age would not be much different from half of its age (half of ~10 Gyr, or somewhat higher), and only about 10% or less of low-luminosity stars in a sample might be as young as the empirical fit implicitly assumes. Fortunately, also, the tracks for 1 and 10 Gyr stay much closer together over the interval of interest. Hence a second way of doing the *M-L* transformation is to assume that the theoretical tracks are correct, that most of the stars have ages of order 1 or 10 Gyr, and to use one of these sets or their mean to assign masses.

Very different slopes of the IMF near the hydrogen-burning mass limit will be derived from a given LF using empirical and theoretical transformations. This point has been discussed in greater detail in D'Antona and Mazzitelli (1986), Reid (1987), Liebert and Probst (1987), and Kroupa, Tout, and Gilmore (1990). In the following discussion, the statement that the derived IMF shows an upturn means that the number density per unit interval in log mass increases with decreasing mass. Due to the

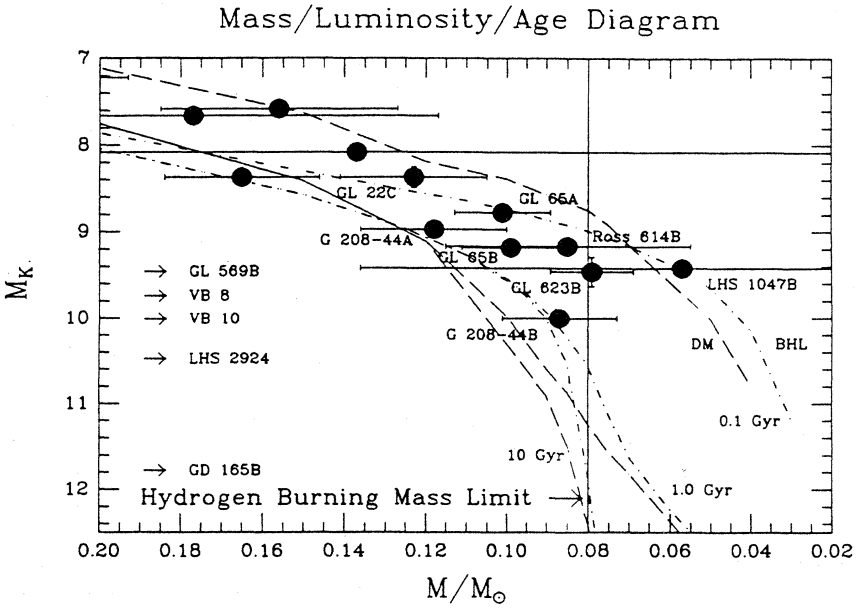

FIG. 21. Mass-luminosity-age diagram for very-low-mass objects. The isochrones of D'Antona and Mazzitelli (1985, DM, dashed curves) and Burrows *et al.* (1989, BHL, dot-dashed curves) are shown for ages of 0.1, 1.0, and 10 Gyr. The seven lowest-luminosity red objects known with determined masses are within the speckle survey, and the four least massive are brown dwarf candidates. Other brown dwarf candidates are shown on the left at their respectively M_K's. Taken from Henry (1991).

sharp curvature of the theoretical tracks of Fig. 21—in contrast to the linear empirical law—it is possible for the IMF to show an upturn near the stellar mass limit when the LF shows a downward slope. This is due to the fact that, as the theoretical curve increases in slope, smaller intervals of mass correspond to the same interval in luminosity; thus a given number of stars in this luminosity interval transforms to a larger number for a fixed mass interval.

3. Proper-motion surveys

A proper-motion survey is conducted by comparing the position of stars on photographic plates taken at two different time epochs. The great majority of faint stars will be distant enough to show no perceptible motion and can therefore serve as a suitable positional reference frame for the few that do show motion. Such surveys have been very efficient at culling out nearby stars of the galactic disk population, as well as high-velocity interlopers from the halo population. Only those using large Schmidt telescopes reach faint enough over large areas of the sky so that they might possibly include massive, young brown dwarfs of luminosities that are similar to those of the faintest main-sequence stars.

The most important survey to date was carried out by Luyten (1963) using plates taken with the Palomar 1.2-meter Schmidt. This was the first such survey carried out with a specially constructed automatic measuring machine. The combination of using red plates, a very faint limiting magnitude ($m_R \sim 20$), and a small motion limit (the proper motion, $\mu \geq 0.1''$/yr) resulted in the discovery of very-low-luminosity stellar objects. A catalog and finding charts have been published for the ~ 3600 stars with measured proper motions larger than $0.50''$/yr (Luyten, 1979a, 1979b). Dawson (1986) finds this portion of the survey 90% complete for $m_R < 18$ over 65% of the sky. Only a catalog is available for the $\sim 50\,000$ stars with $0.2 < \mu < 0.5$ arc sec/yr (Luyten, 1979c). A more complete discussion of these and other proper-motion catalogs is found in Reid (1987) and Liebert and Probst (1987), who discuss their use in constructing the luminosity and initial mass functions of VLM stars.

New proper-motion surveys are already under way using the new Palomar Sky Survey conducted since the mid-1980s. These plates, utilizing finer-grained emulsions, will result in improved positional accuracies and limiting magnitudes.

These luminosity and mass functions are constructed from samples selected for particular intervals of proper motion and, hence, are vulnerable to bias based in some complicated way on the space motions of the stars. Brown dwarfs detectable at these optical wavelengths might be expected to have small mean tangential velocities, since they should be young. (The velocity dispersions of stars are known to increase with increasing age.)

Despite the possibility that some stars having very low tangential velocities may have been missed, the proper-motions surveys have been very efficient at identifying the nearest neighbors to the Sun and in finding a large fraction of the intrinsically faintest stars currently known, some of which might be brown dwarfs. The sample of solar neighbors is optimum for study for several reasons: Their distances and, hence, luminosities may be directly measured by trigonometric parallaxes. They are the brightest objects of a given class for all follow-up observations. Perhaps most importantly, they are also the sample most amenable to the discovery of fainter, close companions, a key component of the search for brown dwarfs.

The least luminous of the well-studied solar neighbors currently are two stars cataloged in Luyten (1979a) as LHS 2924 and 2065, each with distances determined from accurate trigonometric parallaxes (Monet *et al.*, 1992). The inferred absolute visual magnitudes (M_V) are fainter than $+19$, implying luminosities of a few $\times 10^{-4} L_\odot$ (Fig. 19). Such luminosities indeed place them very close to the limiting mass for hydrogen burning (see Sec. II.F). As also discussed in Sec. III.A.1, it is also possible that either or both are brown dwarfs.

4. Optical and infrared color surveys

The red colors of the lowest-mass stellar objects provide a selection method free of kinematical bias. With the availability of sensitive emulsions, automated measuring machines, and sophisticated computers, very large color surveys covering large areas of the sky have been carried out to produce luminosity and mass functions which may also penetrate the substellar regime. Historically, this method has been fraught with danger, since small systematic errors in the calibration of photographic colors, or in the assignment of absolute magnitudes (luminosities) based on photometric colors, have resulted in large systematic errors in the LFs, the space densities of low-luminosity stars, and in the IMFs. More recently, however, the reddest, best candidates for very-low-luminosity objects have been checked with follow-up infrared and optical photometry and spectrophotometry.

Gilmore and Reid (1983) and Gilmore *et al.* (1985) presented the first large samples of stars selected on the basis of V and I colors. Relatively few very-low-luminosity candidates were found, and they argued that the LF and IMFs turn downward at masses below $0.3 M_\odot$; but these authors used an empirical M-L calibration (see Sec. III.A.2). Using a theoretical M-L relation which featured an inflection point in the luminosity near this mass due to opacity effects, Kroupa, Tout, and Gilmore (1990) found that the IMF need not reach a maximum near $0.3 M_\odot$. They argued that the available observations did not rule out either rising or declining slopes, but that the most likely slope was fairly flat.

Hawkins (1986) showed that one could reach to greater limiting volumes by using the same technique with R and I colors. Hawkins and Bessell (1988) and Leggett and Hawkins (1988) extended the scope of this work and

featured follow-up (especially infrared) observations of the reddest candidates. Their derived IMF's showed upturns as they approached the stellar mass limit. Presumably, some of their reddest candidates could be brown dwarfs, and, in any case, the extrapolation of these results to substellar masses would imply a large space density of brown dwarfs. Photometric parallaxes were derived based on comparisons of colors and spectra to those of the "benchmarks" with trigonometric parallaxes discussed in the previous paragraph. (For a more general discussion of the observational calibrations, see Bessell, 1991.) Proper-motion measurements were also reported for the color-selected stars in the Hawkins and Bessell paper. If the motions and assigned distances are correct, the space motions are small, implying that the coolest stars are a relatively young population.

Reid (1987) reviews the apparently discrepant conclusions of the Gilmore and Hawkins groups and concludes that the preponderance of evidence favors an upturn in the mass function near the stellar mass limit. Earlier, this conclusion had been advanced by D'Antona and Mazzitelli (1986) using what were then new interior models to convert the luminosity to a mass function. However, the most recent analysis to have been published at the time of this writing is that of Tinney, Mould, and Reid (1992), which utilizes six fields from the new Palomar Sky Survey for which follow-up infrared and optical photometry is complete. These authors find stars red enough to reach $\log L/L_{\odot} = -3.5$ if they are main-sequence objects, but the indicated mass function is flat near the substellar limit. It may nonetheless be concluded from *all* the above studies that large numbers of brown dwarfs should exist, unless for some unknown reason the star formation process terminates at masses very near the hydrogen-burning limit. It is unlikely that the contribution of brown dwarfs adds substantially to the local mass density of the galactic disk (Kroupa, Tout, and Gilmore, 1990; Tinney, Mould, and Reid, 1992).

Other color surveys whose conclusions are just being finalized are Ph.D. dissertations (Jarrett, 1992; Kirkpatrick, 1992). The former uses the Ophiuchus and Taurus clouds as opaque screens, in order to search for genuinely red foreground dwarf stars in the galactic plane. The latter utilizes photometric data from J. T. McGraw's CCD Transit Instrument, a survey of a strip of the sky at fixed declination.

In addition to their red colors, the M dwarf stars show strong, broad spectral features, recognizable even at low spectral resolution. Many early surveys therefore used objective prisms to identify these stars in large photographic fields, following Vyssotsky (1963). Most recently, a very cool stellar object—PC 0025+0447—has been found serendipitously by Schneider *et al.* (1991) in a deep objective grism survey with a CCD detector on the Palomar 5-meter reflector. The primary goal of this survey is the discovery of high-redshift quasars. This object shows redder colors and later-type optical and infrared spectra (Graham *et al.*, 1992) than any field object yet found, though not as red as the companion object GD165B discussed in Sec. III.C.2. Its most remarkable property, however, is the extraordinary emission line due to Balmer alpha. Speculations as to the origin include an unprecedented degree of chromospheric activity at the surface of the star and some kind of interacting binary system. The luminosity of the system remains unknown, pending measurement of a trigonometric parallax.

Until recently, infrared survey work on the field population had not been possible, despite the fact that these stellar objects emitted most radiation longwards of 1 μm. Since the deployment of sensitive infrared array detectors, the surveys for field objects have been focused on the specific fields of young clusters and star-forming associations; these results will be discussed in Sec. III.B. Surveying of large portions of the sky has not been possible with existing configurations.

The all-sky survey of the Infrared Astronomy Satellite (IRAS) did not yield any brown dwarfs from 5776 sources detected at 12 μm in the Point Source Catalogue (Beichman *et al.*, 1990). However, at these far-infrared bandpasses, IRAS would have been able to detect brown dwarfs of temperatures 1000–3000 K out to distances of only a few parsecs.

A deep all-sky survey in the 1–2 μm bands, on the other hand, could be a powerful way of finding field stellar objects at low temperatures. For example, a proposal to use dedicated 1-m telescopes with current infrared array detectors aims to reach a limiting magnitude of 14 at 2.2 μm (Kleinman *et al.* 1991). This would permit 2500 K objects to be detected out to 50 pc, and 1000 K brown dwarfs to be found at 7 pc. The sensitivity of such a survey would be greater than IRAS for even cooler objects with temperatures above 500 K.

B. Searches in young clusters and star-forming regions

Focusing a survey for substellar objects on a young stellar aggregation offers some obvious advantages. First, the objects will be young and hence relatively luminous. Secondly, they have at least approximately the same ages, so that it will be possible to assign masses based on estimates of the luminosity alone. Furthermore, they all lie at the same known distance. Finally, there are several interesting aggregations close enough for observation, ranging from molecular clouds forming stars of the order of 10^6 to 10^7 years old to clusters as old as 10^9 yr. Exploitation has been made possible by the development of efficient infrared array detectors.

There are drawbacks as well. Star-forming regions may be in the galactic plane, so that heavily reddened background stars may be confused with genuinely cool members of an association. Newly formed stars may possess remnant accretion disks, large rotation rates, and corresponding chromospheric and coronal activity, which might distort their spectra and colors. Furthermore, there is evidence of considerable variation in these properties among stars in the same cluster. In very young systems, the assumption of spherical symmetry

may break down, which greatly complicates the task of calculating accurate theoretical tracks and comparing with observations. Moreover, we cannot necessarily assume that a group of objects is coeval. The age spread in a giant molecular cloud may be significant compared to the mean age. These difficulties are likely to be magnified for the youngest populations, but these are the very cases in which brown dwarfs are expected to be most luminous!

Perhaps the biggest kind of drawback is a set of practical problems related to the faintness of the candidates and the distance to the cluster; much more information may be gained, for example, about field stars in the solar neighborhood. Usually the available information is restricted to photometry in a few passbands. These must be converted to T_e and luminosity based on a calibration and the estimated distance of the cluster or group. For example, several of the groups discussed below used the temperature scale of Berriman and Reid (1987) to convert their observed colors. This scale is based on blackbody fits to energy distributions and infrared spectra of nearby dwarf stars. Despite the recent criticism by Stringfellow (1991), this scale is a valid representation of their assumptions and observational data on nearby stars (see Berriman, Reid, and Leggett, 1992). It nonetheless consistently places disk stars to the right of the HR diagram positions of most theoretical models for ages $\geq 10^9$ yr. A new scale based on an attempt to fit optical and infrared spectrophotometry with synthetic spectra of model atmospheres (Kirkpatrick, Kelly, *et al.*, 1993) would shift the temperature scale a few hundred degrees warmer [see also the Becklin and Zuckerman (1988) data points in Fig. 19]. In any case, if the predominantly old disk stars are made to match the theoretical predictions, then the cluster candidates would be shifted towards higher mass.

Finally, even after the cluster/association candidates are placed in a true HR diagram, there remain a variety of theoretical calculations from which to choose. Their different predictions as to L and T_e for a given age and mass are attributable to different physical assumptions in the same group (explored comprehensively in Burrows *et al.*, 1989), as well as to differences in the codes among different groups supposedly making similar physical assumptions.

1. The Taurus-Auriga clouds

One of the nearest sites of recent star formation is this loose association. Numerous low-mass, pre-main-sequence objects have been found in optical and x-ray surveys, including many T Tauri and post-T Tauri objects with a characteristic age of 10^6 years. In an effort to detect lower-luminosity companions to 26 of these known objects, Forrest *et al.* (1989) carried out a 2.2 μm (K-band) imaging survey, covering areas of 25 arc sec square near each target. Of the 20 new objects detected at $K \sim 13-16$, nine were found to have exceptionally red JHK colors; moreover, four of seven objects found to be visible on first-epoch Palomar Sky Survey plates had proper motions indicative of membership in the association. For the estimated distance of 140 pc, the luminosities of the objects as members would be only of the order of $10^{-3}L_\odot$; for an age of 10^6 yr, the inferred masses would be near $0.01M_\odot$. The large and random separations of the very red objects from the T Tauri imaging targets indicated that they should generally be single "free floaters" rather than binary companions. The inferred population of low-mass brown dwarfs in Taurus would be quite large.

Follow-up spectroscopy, however, has revealed that most of these candidates do not have spectra consistent with their having very low temperatures (Stauffer *et al.* 1991). Instead, they may be background M dwarfs and stars of even earlier spectral type, distant and heavily reddened. In retrospect, the large and highly variable extinction in the background rendered the interpretation of the detected sources very difficult. Thus, while the Taurus-Auriga region remains a fertile potential hunting ground, there is as yet no strong evidence for a large brown dwarf population.

2. The Rho Ophiuchus molecular cloud/cluster

Rho Ophiuchus differs from Taurus-Auriga in having such a high internal extinction ($A_v > 50$ in the core) and stellar density that relatively few background sources are likely to be detected. This may be a bound cluster in the process of formation and includes high-mass stars. Its close proximity (160 pc) and relatively young age ($< 3 \times 10^6$ yr) suggest that this cluster will be a fruitful place to search for low-mass stellar objects. The question is how deep one can look into this cloud complex as a function of the object's luminosity. Rieke, Ashok, and Boyle (1989) surveyed a modest field to a limiting K magnitude of ~ 14 and found no new sources over and above those found in the previous study of Wilking and Lada (1983) to $K \sim 12$. Another survey to $K \sim 14$ over a larger area detected 35 new sources (Barsony *et al.* 1989), though there was no indication any of these were substellar.

A deeper search ($K \sim 15$) by Rieke and Rieke (1990) produced several brown dwarf candidates from the preliminary analysis. These authors (Comeron, Rieke, Burrows, and Rieke, 1993) have now completed the survey of 200 square arc min in the cores of the Rho Ophiuchus clouds. Completeness of $K = 15.5$ and H (1.6 μm) $= 17$ is achieved. They have detected 91 faint sources, all with multiple measurements usually in both bandpasses, some as faint as $K = 17.5$. Since minimal background contamination is expected, it was assumed that each of these would fall on a theoretical isochrone for an age of (up to) 2×10^6 yr, and a unique value of extinction for each object could be found consistent with this assumption. Intrinsic luminosities were thus derived and masses appropriate to each luminosity were found. Perhaps seven objects have luminosities low enough for masses below $0.05M_\odot$ to be inferred. The IMF distribution appears to be continuous across the substellar boundary with a power-law exponent of roughly -1.3.

3. The Pleiades

The most attention in infrared searches for substellar candidates has been devoted to the Pleiades cluster, with an age, estimated from the main-sequence turnoff, of $6-7\times10^7$ yr. However, Stauffer (1984) and others have made the case that some low-mass stars in the cluster may be significantly older, perhaps as much as 10^8 yr. Moreover, the distance of the cluster has been called into question: Early determinations clustered around 125 pc, while a recent trigonometric parallax study with a new instrument yielded about 150 pc (Gatewood *et al.*, 1990). With the smaller, early infrared arrays, the initial efforts again focused on finding low-luminosity, resolved companions. Skrutskie, Forrest, and Shure (1986) and Zuckerman and Becklin (1987) found no substellar companion candidates around main-sequence and white dwarf members of the cluster, respectively. However, in this cluster of low internal extinction, the larger-format CCDs could also be used to search for low-luminosity single members. Jameson and Skillen (1989) and Stauffer *et al.* (1989) covered some 125 square arc minutes at R and I and 900 square arc min at V and I, respectively. In both cases several very faint, red sources were found in the part of the color-magnitude diagram expected for brown dwarfs or VLM stars. Since their LF peaked near $0.2M_\odot$, Stauffer *et al.* (1989) did not find evidence that brown dwarfs were a major component of the Pleiades.

More extensive and deeper studies of the Pleiades have since led to different and perhaps contradictory conclusions. Hambly and Jameson (1991) used R and I Schmidt photographic data to study a three-degree diameter region—encompassing the core of the cluster. This study provides a nice illustration of the complexity of a comprehensive photographic investigation covering multidegree fields using an automatic measuring machine. Some 140 000 to 180 000 raw stellar images from each of two pairs of IIIaF (R) and IV-N (I) plates had to be identified and matched with counterparts at the same position on the other plates. The procedure had to cope with both extended objects (galaxies), blended images, and plate flaws due to such things as diffraction patterns around bright stars. The authors excluded from consideration fields around bright stars. The photographic R and I magnitudes had to be calibrated in terms of the R,I photometric systems, a somewhat complicated task for objects of red color because of differences between the R passbands of the photographic and photometric detectors. Objects corresponding to the locus of the main sequence and its theoretical extension to substellar masses at the Pleiades age were identified in an R, R-I diagram; this means that the theoretical model loci (L, T_e) had to be converted to these colors using the relations of Berriman and Reid (1987) for photometric R,I. The photographic point sources found in a band around the main-sequence and predicted brown dwarf loci were treated as low-mass Pleiad candidates. The numbers of candidates in a given I magnitude bin in the core of the cluster were compared with those measured from an annulus around the cluster, assumed to be representative of the background. The luminosity function was then assembled from the difference in these counts per unit surface area. The initial mass function was then constructed from the theoretical isochrone for 6×10^7 yr, which predicts a mass for a given luminosity. The resulting mass function was flat or rising slightly down to the stellar mass limit. A lower limit of 30 brown dwarfs was found in this statistical manner, but it is not known from this study alone which are actually Pleiades objects and which are background stars. Moreover, a large number of faint objects were detected only on the I plates, and these could include many more potential brown dwarfs among the great majority which will be background stars.

The same group (Hambly, Hawkins, and Jameson, 1991) has complemented the above investigation of the Pleaides with an astrometric survey, measuring Palomar Sky Survey plates from the 1950s as the first epoch. Fortunately, the Pleiades cluster has a quite distinct proper motion, so that contamination from the field does not pose an overwhelming problem. The lower main sequence is obvious in an I, R-I diagram of the objects with the cluster motion, and it extends to at least $M_I=11.5$. Even with fairly reliable criteria for identifying the cluster members, problems remain with the construction of a luminosity function and an initial mass function and with their interpretation. These include (1) the fact that even red colors can be affected by intense flaring activity, a characteristic of low-mass Pleiads, (2) significant uncertainty in the distance of the cluster, (3) doubt as to whether the lower-mass stars could have substantially older ages, (4) significantly different theoretical mass-luminosity relations for the standard age of $6-7\times10^7$ yr depending on the theoretical source, and (5) incompleteness for the faintest and most interesting magnitude bins, those affecting the IMF below $0.1M_\odot$. This group's LF appears, nonetheless, to peak at $M_I\sim9.5$, similar to that found by Stauffer *et al.* (1989) and as may occur for the LF of the field galactic disk. Whether the mass function declines below $0.2M_\odot$, and whether there are any bona fide brown dwarfs among the sample of fainter cluster members, remains uncertain.

The deepest survey of the Pleiades thus far is that of Simons and Becklin (1992), who imaged some 200 square arc min at both the I and K bands using a CCD and infrared array. Candidates were thus identified by comparison of position in an I, I-K diagram with a theoretical isochrone for 10^7 yr. A reference field of 75 square arc minutes was used to estimate the contribution of background stars, and the authors showed that the two fields had the same general stellar count rates at the relevant magnitudes, though the authors calculated that the Pleiades field showed an excess of 22 ± 10 objects within the designated isochrone band. The range of I magnitudes corresponded to masses in the range $0.04-0.1M_\odot$, so that there was little overlap with the photographic studies discussed previously. However, the correspond-

ing mass functions do not agree at $0.1M_{\odot}$; the Simons and Becklin study predicts a total of ~3400 objects in the above range in the entire cluster.

The Simons and Becklin (1992) survey is potentially the most interesting so far in the Pleiades, because the depth should clearly penetrate well into the brown dwarf regime. The problem is that, for such faint objects, it will be difficult to garner conclusive information about the parameters of the candidates. The assignment of masses depends somewhat on which theoretical model set is adopted to construct the relevant isochrone, as discussed at the beginning of Sec. III.C. They also depend on the Berriman and Reid (1987) scale for their conversion of $(I\text{-}K)$ to T_e. There is some dependence also on the age and distance assumed for cluster members.

4. The Hyades

This is the oldest (6×10^8 yr) and closest (~45 pc) of the stellar aggregations searched for substellar constituents. Any member brown dwarfs should therefore be fairly dim, but well behaved, as measured rotation rates for VLM Hyades dwarf stars do not exceed 20 km/sec (Stauffer, Hartmann, and Latham, 1987); thus, the induced coronal and chromospheric activity is modest enough not to affect seriously the behavior of the photospheres. Hubbard *et al.* (1990) and Stringfellow (1991) have noted that the Hyades is sufficiently old that the LF should separate into distinct lower main-sequence and brown dwarf components. Due to the size or relative looseness of the cluster—and, ironically, its proximity to the Sun—it is difficult to establish membership reliably from proper-motion measurements alone. Moreover, a new astrometric study (Reid, 1992) shows evidence for mass segregation in this old cluster: thus the lower-mass stellar objects may be less centrally concentrated (and may also have escaped more easily) than the higher-mass stars.

Leggett and Hawkins (1988, 1989) selected field stars with large R-I colors for follow-up infrared (JHK) photometry and derived infrared luminosity functions. A peak in the LF near $M_K=+6.7$ corresponded to $\sim0.2M_{\odot}$, near the value often claimed for a low-mass peak in the disk IMF (cf. Scalo, 1986). A comparison of theoretical isochrones with the observed data sets found no evidence of a rising mass function near the stellar mass limit or of a bifurcated LF indicative of a brown dwarf population (Hubbard *et al.*, 1990). The dimmest several of these candidates might still be substellar, if Hyades members. Unlike their brighter counterparts, however, these are so faint that there is as yet no astrometric information.

Bryja *et al.* (1992) identified several faint, red objects on multiple epochs of red Palomar Sky Survey plates and suggested that they were candidate brown dwarf or VLM stellar members of the cluster based on proper-motion measurements. The JHK colors are somewhat inconclusive, while optical ($BVRI$) colors are anomalous or suggestive of higher temperatures. Spectroscopic observations are being attempted to clarify the situation. Reid's (1992, and in preparation) comprehensive color/astrometric survey for Hyades members should help clarify the nature of the faintest of the Leggett and Hawkins and Bryja *et al.* candidates.

Finally, I- and K-band imaging of fields around 49 known Hyad stars has resulted in the identification of a sequence of VLM/brown dwarf candidates (Macintosh *et al.*, 1992). Proper-motion measurements should help demonstrate whether they are components of wide binary systems or field members of the cluster.

C. Discovery and analysis of substellar companions

For stellar objects in close binary systems, the masses may be determined directly by analysis of the binary orbits. The observational techniques may include direct photography of visual binaries near enough to the Sun (or more distant ones that can be imaged from space), astrometric perturbation analyses and speckle interferometry for barely resolvable pairs, and/or spectroscopic measurements of radial velocities for unresolved and close pairs. By establishing the mass, such studies offer the best hope for unambiguous identification of a substellar companion to a nearby star. Results from these and other techniques applicable to more distant companions are discussed next.

1. Wide optical companions with common proper motion

Photography of the fields around nearby stars has been employed for decades to discover resolved companions sharing the space motion of the primary. Several early "benchmark" stars of very low luminosity were found in a survey of known solar neighbors by van Biesbroeck (1961); vB8 and vB10 are among the best known of these. The latter, at $M_V\sim+18.7$, was the least-luminous known star until the 1980s.

2. Infrared imaging and photometry

Continuation of the search for fainter, resolved companions in recent years has been carried out at infrared wavelengths, using new generations of wide-format infrared array detectors. Searches for companions to stars in young clusters and associations were mentioned in Sec. III.B; here we focus on companions to nearby field stars of the galactic disk, closer and easier targets. Jameson *et al.* (1983) scanned 21 nearby stars at 1–2 μm (JHK bands), but found no resolved companions at least 10 arc sec from the primary star. Skrutskie *et al.* (1989) conducted a more extensive search, but found only one brown dwarf candidate, a resolved companion to BD+16°2708=Gliese 569 (Forrest, Skrutskie, and

Shure, 1988). However, these authors concluded that Gl 569B could also be a VLM star, though it is significantly more luminous than vB10 and appears to be cooler than known VLM stars of similar luminosity (Henry and Kirkpatrick, 1990).

G. H. and M. J. Rieke have surveyed all known stars within 8 pc of the Sun, north of -20 degrees declination and fainter than $M_V=+11$ (early M spectral type). The search had a detection limit of $K(2.2\mu)=15.5$, corresponding to at least six magnitudes (a factor of 250 in flux) fainter than vB10 and covering fields of radius >100 astronomical units (AU) around each star. No plausible brown dwarf candidates were found.

If the companion cannot be spatially resolved from its primary star, there appears to be no simple way to deconvolve the binary components, if both are low-mass stellar objects (Probst, 1981). However, Probst (1983a, 1983b) realized that if the primary star were a white dwarf—a low-luminosity object of substantially higher temperatures—then a range of low-mass stellar companions and even a moderately cool brown dwarf ($T\geq 1000$ K) might be detected at infrared wavelengths. Using broadband 1–2 μm (JHK) photometry—the technology of the early 1980s—Probst, nonetheless, failed to find any companions in observations of approximately 100 field white dwarfs.

Zuckerman and Becklin (1987a) continued the search of white dwarf stars for infrared excesses, first concentrating on those stars in the relatively young Pleiades and Hyades clusters where any brown dwarf companions might be more luminous than the norm. None of the 14 cluster white dwarfs showed an excess. These authors also initiated a much broader survey of field white dwarfs, using infrared array detectors so that they might find both unresolved and resolved companions.

Two exciting discoveries resulted from this search. First, Zuckerman and Becklin (1987b) found that the pulsating white dwarf G29-38 (=ZZ Psc) showed an infrared excess. Initially, the simplest explanation was that the star had an unresolved companion with a color temperature of about 1200 K and a luminosity of $5\times10^{-5}L_\odot$; these are values much lower than any low-luminosity star. However, Graham, Matthews, *et al.* (1990) and Tokunaga, Becklin, and Zuckerman (1990) detected flux at 10 μm in an amount far more than predicted by the thermal energy distribution of the hypothesized companion. These authors argue that the infrared excesses at all wavelengths might more plausibly be attributed to some kind of dust shell around the white dwarf (see also Patterson *et al.* 1991). On the other hand, Graham, McCarthy, *et al.* (1990) found that the radial velocity of the star may vary at the 5–10 km s^{-1} level. Follow-up observations by Barnbaum and Zuckerman (1992) indicate that the variations are probably real with a period near 11 months, which leaves open the possibility that G29-38 has a low-mass companion (see also Zuckerman, 1992).

Second, Becklin and Zuckerman (1988) found a resolved companion to a second white dwarf, GD165. At a distance corresponding to some 120 AU from the primary star (on the plane of the sky), this component has a color temperature (2100 K) and luminosity (7.8×10^{-5}) making it the coolest and dimmest detected brown dwarf candidate. It also exhibits a very late type and unusual spectrum (Kirkpatrick, Henry, and Liebert, 1993). Even so, depending on the precise values of these parameters and the theoretical models used in the comparison, GD165B might still be a stellar object near $0.07-0.08M_\odot$ (Burrows *et al.* 1989; Greenstein, 1989a, 1989b). Moreover, plausible brown dwarf tracks of $60-65M_J$ through this position on the HR diagram (Fig. 19) imply that the companion is younger than about 10^9 yr. Yet the 11 000 K white dwarf has a cooling age of about 6×10^8 yr, before allowing for a nuclear-burning lifetime. This constraint requires the white dwarf to have evolved from a massive progenitor star, with upwards of $5M_\odot$. GD165B remains one of the best brown dwarf candidates, but even its credentials are not unambiguous.

However, with the completion of the survey of approximately 200 white dwarfs, Zuckerman and Becklin (1992) find a luminosity function of companions that includes many low-mass M stars, but very few, if any, below the stellar mass limit of $0.075-0.08M_\odot$. The primary stars of the binaries in this sample should have had masses near or above $1M_\odot$. A complementary sample is formed by the astrometric and infrared speckle work on stars in the solar neighborhood, since these are nearly all well below $1M_\odot$.

3. Photographic, astrometric perturbations and orbit determinations

The existence of an invisible, close companion to a nearby star may be inferred from the discovery of periodic perturbations in the position of the primary star, as first demonstrated in Bessel's (1845) discovery of the white dwarf companion to Sirius. Photographic plate sequences of nearby stars spanning many decades have been obtained at the Sproul Observatory and more recently at the U.S. Naval Observatory. Reviews of these results may be found in Lippincott (1978), Harrington (1986), and van de Kamp (1986). While many low-mass stellar companions and objects near the limit have been discovered in this manner, it has been difficult to establish the reality of many of the perturbations and which of the real companions have substellar masses (Heintz, 1978). One of the longest-studied cases is Barnard's star, the Sun's nearest neighbor after the Alpha Centauri system. Van de Kamp's (1977, 1981) suggestion of one or two Jovian companions has found no support in the independent analyses of Gatewood and Eichhorn (1973) and Heintz (1978).

Another interesting astrometric system which differs in having two components resolved, but quite low in mass, is Wolf 424. Heintz's (1989) analysis suggests that both are, in fact, substellar, with estimated masses of 0.05 and $0.06M_\odot$. The accuracy of this kind of analysis is difficult

to assess, since it depends on the precision with which the positions and separations of two faint stellar images can be measured on old Sproul Observatory plates spanning 50 years. A detailed speckle interferometric, photometric, and spectroscopic study by Henry *et al.* (1992) suggests that the orbital solutions of Heintz (1989) may be in error. That the objects are substellar is not supported by the infrared spectroscopy of Davidge and Boeshaar (1991).

Considerable improvement can be made in astrometric measurements at optical wavelengths by using new telescopes and optics designed for this purpose, by locating them in modern thermal enclosure sites ("domes") with excellent atmospheric seeing, and by using more accurate and sensitive detectors.

4. Infrared speckle interferometry or imaging

As the size of a telescope aperture increases, the instantaneous image of a point source breaks into smaller sections, into a distribution of what are called "speckles," due to the disturbance of the wave front as it passes through the Earth's atmosphere. Labeyrie (1970) first pointed out that individual speckles contain spatial information on a source to the diffraction limit. The theory and application of speckle interferometry at optical wavelengths is discussed by Dainty (1984) and Roddier (1988). McCarthy (1976) pioneered the application of speckle interferometry at infrared wavelengths.

The infrared speckle interferometric technique has been used to search for low-luminosity companions to all M dwarfs known within 8 pc of the Sun, north of $-25°$. M dwarfs have masses up to about $0.4M_{\odot}$. The search annuli correspond to about 1–10 AU separations on the plane of the sky. These results are reported in the Ph.D. dissertation of Henry (1991). The remainder of this section, with the exception of the comments in the last two paragraphs, has been extracted from these references.

Six new companions were found, and masses were determined which ranged from 0.39 to $0.05M_{\odot}$. Three of the new companions—G208-44B, Gliese 623B, and LHS 1047B—and one previously known secondary to a survey star, Ross 614B, are brown dwarf candidates. These and other candidate field brown dwarfs are listed in Table II. However, the error bars on the mass determinations of all four cases allow the true masses to be above $80M_{\rm J}$ ($0.08M_{\odot}$). Infrared photometric observations allow the luminosities of these objects to be estimated for an empirical *M-L* relation (see Fig. 20, taken from Henry, 1991). Three of the four candidates can be explained theoretically either as substellar objects with ages of the order 0.1 Gyr or as stars above the mass limit with ages of 1–10 Gyr. The dimmest of these objects, G 208-44B at $M_K \sim +10$, cannot be as young as 0.1 Gyr, but might still be a marginal brown dwarf. Even so, note that it is significantly more luminous than the faintest single stars like LHS 2924, discussed in Sec. III.A.3, and a factor of 5 more luminous at 2.2 μm than the companion to the white dwarf GD165 (Sec. III.C.2).

The luminosity function of the local sample of 99 nearby low-mass stars, including the companions, appears fairly flat in a histogram of number versus half magnitude intervals in M_K (Fig. 22). The numbers decline sharply at $M_K = +10.0$. This result implies two things: (1) The very faintest known stellar objects in the field are rare enough not to be represented in the known sample within 8 pc of the Sun, and (2) companions fainter than $M_K \sim +10$, like GD 165B, are relatively rare. There is, however, no reason to assume that the known sample of single stars and companions is complete to 8 pc, and it is, of course, the dimmest cases that are most likely to have been missed.

TABLE II. Brown dwarf candidates and lowest-luminosity VLM stars.[a]

Name	K	J-K	M_K	Mass ($M_{\odot}$)	Spectral type
(a) Field stars and very wide binary companions					
GD165B	14.09	1.66	11.78		>M9
LHS2065	10.75	1.26	10.31		M9
LHS2924	10.68	1.17	10.48		M9
GL 569B	9.65	1.13	9.55		M8.5
PC0025+0447	14.93:	1.24			M9.5
(b) Unresolved companions					
G29-38B?	13.45		12.70		
HD114762B				>0.011	
(c) Companions with astrometric mass determinations					
G208-44B	8.28	1.06	10.00	0.087±0.014	
GL 623B	8.85	1.13	9.46	0.079±0.010	
LHS 1047B	8.04	1.01	9.42	0.057±0.079	
Ross 614B	7.24	1.09	9.17	0.085±0.030	

[a]Data taken from Henry (1991); Kirkpatrick, Henry, and McCarthy (1991); Latham *et al.* (1989); Schneider *et al.* (1991); Becklin and Zuckerman (1988); James Graham (1993, private communication).

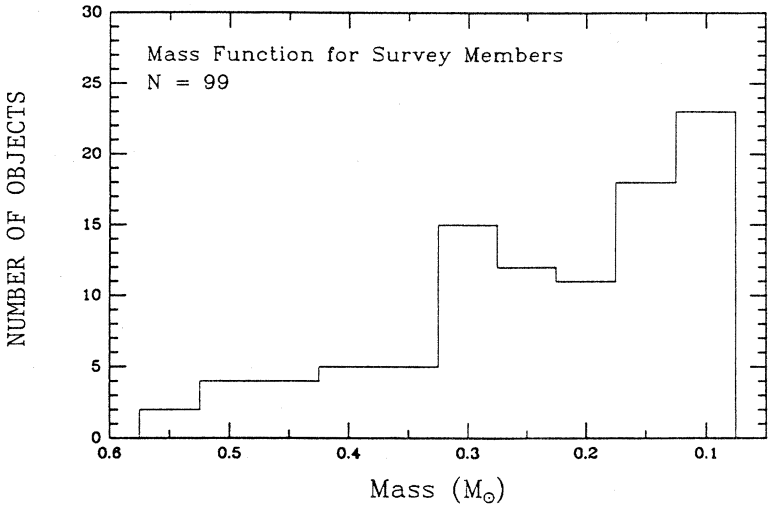

FIG. 22. Mass function for all objects in the survey, grouped in bins of $0.05M_\odot$. Taken from Henry (1991).

The empirical, linear relation derived from the data of Fig. 20 and other sources was then used to estimate masses for all stars in the local sample, including the binary components (which have large individual errors). The result is the estimated IMF for the VLM's in the solar neighborhood (Fig. 22) from the empirical method (Sec. III.A.2). Like many similar IMF determinations for single stellar objects in field and cluster populations, a rising number density with decreasing mass is inferred down to the stellar mass limit. It would rise faster if an *M-L* transformation from theory had been used instead.

5. Radial velocity surveys

A complementary technique to the various imaging approaches for finding unresolved companions to nearby stars is to search for radial velocity variations due to orbital motion of a visible component. The stars need to be bright enough for precise, high-resolution line profiles to be measured.

The most comprehensive search to date of Marcy and Benitz (1989) covered 70 low-mass M dwarfs, some 80% of all known single stars later than dM2, brighter than $V=10.5$, and accessible to observation from Northern Hemisphere observatories. Since the brightness constraint generally required the stars to be within 10 pc, there is considerable overlap with the infrared speckle sample described previously. While the velocity searches are sensitive to smaller orbital separations, variations in the primary out to at least a few AU could be measured and overlap with McCarthy and Henry might occur if the secondary is detectable in the infrared. Marcy and Benitz (1989) uncovered only one companion that is possibly substellar—to the star Gliese 623 (Marcy and Moore, 1989)—and it was independently discovered in the infrared speckle work. Like several stars in the sample analyzed with the speckle technique, this star has a possible mass range ($0.067-0.087M_\odot$) that straddles the cutoff mass for hydrogen burning. When these and the results of the complementary astrometric searches are considered together, the lack of detections suggests that brown dwarfs with masses above about $0.01M_\odot$ and within about 10 AU of low-mass M stars in the solar neighborhood are rare.

Campbell, Walker, and Yang (1988) employed a special-purpose spectrograph able to measure radial velocities of bright stars to a relative accuracy of 13 *meters* per second. Observations spanning six years of 16 F-K dwarfs and subgiants—stars much closer to the Sun in mass—yielded no inferred companions with masses in the 10–80 M_J range for periods ≤ 50 years. A few stars showed small, but possibly significant, long-term variations indicative of the possibility of planetary companions with masses below $10M_J$.

McMillan (1992) is presently carrying out an even more accurate radial velocity monitoring program with an instrument invented by the late Krzysztof M. Serkowski for this purpose (see McMillan *et al.*, 1985). Standard deviations well below 10 m/sec have been achieved from multiple observations in an observing season. Sixteen solar-type stars have been observed routinely for more than four years, but no conclusive results can yet be announced.

Thus far, the most exciting discovery of these radial velocity searches happened in a somewhat circumstantial manner: Repeated observations of the G dwarf HD 114762 were obtained by Latham *et al.* (1989) in order to establish this star as an accurate radial velocity standard star, under a project for the International Astronomical Union. Instead, they found that this star shows periodic velocity variations with an amplitude of 0.55 km/s and a period of 84 days. The unseen companion has a mass of $11M_J/\sin i$, where i is the angle of inclination between the line of sight and the axis of the orbit. As in any noneclipsing single-lined spectroscopic binary, this inclination angle may not be determined. However, for the system to exceed the $80M_J$ "brown dwarf" upper limit, the inclination must be within 8 degrees of pole on.

A new analysis by Cochran, Hatzes, and Hancock (1991) using even more accurate radial velocity measurements at McDonald Observatory confirms the conclusions of Latham *et al.* (1989). These authors also find an upper limit to the projected rotational velocity of 1 km/s. If the actual rotation rate is similar to that of other F9V main-sequence stars and its rotation axis is nearly parallel to the orbital axis, one concludes that the rotation axis is within 5.7 degrees of the line of sight. This results in the companion mass exceeding the stellar limit. On the other hand, it is possible that HD 114762 is an intrinsically slow rotator and that the companion's mass is substellar.

Some 50 additional stars are being monitored by researchers at the Harvard-Smithsonian Center for Astrophysics, and it is possible that additional variables are being found (Mazeh *et al.*, 1990); the target list includes 24 nearby M dwarfs.

6. Substellar objects in interacting binary systems

Among other binary pulsars, the ablating companion to PSR1957+20 is also known to have substellar mass ($\sim 0.02 M_\odot$), though this is likely the result of its proximity to an energetic source (Fruchter *et al.* 1988). It is also worth noting, if only for completeness, that less exotic interacting binary systems are known in which the secondary component is likely to be substellar in mass. The evolutionary theory of accreting white dwarfs with nondegenerate secondaries predicts that the latter have been whittled down to substellar masses by the time the orbital period of the system reaches the observed minimum near 80 min (Paczynski and Sienkiewicz, 1981). At this point, the secondary becomes a degenerate hydrogen object, and its radius and the orbital period increase with further decreases in the secondary's mass due to mass transfer. Interacting systems with much shorter periods exist in which the secondary is a helium degenerate of substellar mass (Faulkner, Flannery, and Warner, 1972).

D. Searches for halo brown dwarfs

Halo brown dwarfs are predicted to have temperatures below 1000 K (see Fig. 11), making direct detection enormously difficult. Nonetheless, the likelihood that the halo of the galaxy contains a large amount of dark matter (cf. Fich and Tremaine, 1991) has led to widespread interest in the slope of the initial mass function of halo stars near the MMSM (minimum main-sequence mass).

Given that we expect to see only halo objects above the stellar mass limit, one can start by asking if we are detecting halo stars down to approximately the predicted mass. The answer seems to be yes: Monet *et al.* (1992) presented trigonometric parallaxes and estimated bolometric luminosities for the known sequence of high-velocity, metal-poor M subdwarfs in the solar neighborhood; the sequence extends to $\log L/L_\odot \sim -3.0$. If the metallicity of these stars is of the order 0.01 of solar ($[M/H]=-2$), this luminosity corresponds approximately to the position of a $0.1 M_\odot$ model of D'Antona (1987) of this metallicity, a mass just above the substellar limit for this composition. Earlier, Greenstein (1989b) had advanced a similar argument.

The sample of nearby faint halo stars is biased by their kinematic properties, since these are drawn from catalogs of stars with measured proper motions. Nonetheless, interesting estimates from color-selected samples have been made possible by the advent of large-format CCD detectors. Several globular clusters show main sequences extending down to near the limit (Richer *et al.*, 1991, and references therein); in the best case of NGC 6397, the authors estimate that they reach $0.12 M_\odot$. In none of these cluster IMFs is there any evidence of a flattening or turnover in the slope at the lowest masses. Some may have IMF slopes steeper than the Salpeter value long associated with the galactic disk. The authors suggest that brown dwarfs likely exist in large numbers in these clusters.

Richer and Fahlman (1992) have now estimated a corresponding IMF for the field halo population. They faced formidable problems in making this estimate that are not encountered with clusters. First, the much more numerous galaxies and compact extragalactic objects must be eliminated on the basis of having extended images and/or nonstellar colors in V, R, and I. Then, absolute magnitudes and distances must be assigned to each of three-dozen halo star candidates, based on a relation between M_V and the V-I color. M subdwarfs are known to be subluminous in such a color-magnitude diagram, lying up to three magnitudes fainter than their Population I counterparts at a given V-I (see Monte *et al.*, 1992). How subluminous they are is predicted theoretically to depend on the metallicity. Unfortunately, any set of stars in a field halo sample may exhibit a fair range of metallicity, rather than the small dispersion usually found in a globular cluster. This might leave the distance estimates rather uncertain, and the space densities depend on these to the third power. Richer and Fahlman (1992) derive a field star IMF that rises faster than a Salpeter slope, down to about $0.14 M_\odot$. Extension of this slope to $0.01 M_\odot$ would allow VLM's and brown dwarfs to dominate the dark matter content of the galaxy. The expected number density of halo brown dwarfs in the solar neighborhood would be 0.5 objects pc^{-3}.

E. Gravitational microlensing

Paczysnki (1986) first proposed the possibility of observing gravitational lensing events of more distant stars by compact objects in the foreground of our own galaxy. The general idea was to detect invisible "missing" matter, whether in the form of massive black holes or brown dwarfs. Paczynski suggested specifically the monitoring of the light from millions of stars in the Magellanic Clouds in order to detect microlensing events by fore-

ground objects in the galactic halo. The idea of searching for MACHOs (massive, compact halo objects—Griest, 1991) is now being actively pursued by several groups (cf. Griest *et al.* 1991). Paczysnki (1991) and Griest *et al.* (1991) have also suggested that stars in the galactic bulge could be microlensed by similar compact objects of the foreground galactic disk population.

These groups have argued that detectable light modulation should be observable from intervening masses ranging from 10^{-7} to $100M_{\odot}$. The predicted rates are of the order 10^{-7} to 10^{-6} events per star per year for an intervening lens near the stellar mass limit, each of a duration of the order of months or less. The rates are proportional to the lens mass to the $-\frac{1}{2}$ power, while the durations are proportional to mass to the $+\frac{1}{2}$.

For lensing stars located at the optimum distance of about halfway to the galactic center, the size of the Einstein ring of a bulge star's light is similar to the separation of Jupiter from the Sun. Hence Mao and Paczynski (1991) and Gould and Loeb (1992) have pointed out that signatures of Jovian planets in similar orbits around a lensing star would be detectable as short-duration events in the overall light curve.

IV. THE BOTTOM LINE

What is the net result of the application of all of these attempts to find brown dwarfs in the galactic disk population, in young stellar associations, and as companions to bright and nearby stars? First, it has to be said that not a single, unambiguous case of a brown dwarf or planetary companion to a star other than the Sun has been established, with the exception of the cases that likely result from close binary evolution. It should also be clear, however, that many brown dwarf candidates have been found by a variety of methods. The lack of proven examples is due to the great difficulty of establishing accurate masses, temperatures, or ages of the objects.

There is reason to be optimistic that field brown dwarfs might exist in significant numbers. We list some of the best such brown dwarf candidates as of this writing in Table II. The disk population—young and old components—is dominated numerically by low-mass stars, and there is growing evidence that the mass function does not decrease with decreasing mass as it reaches the substellar mass limit. Some of the least luminous objects in various samples may, in fact, be young and substellar, rather than old and above the mass limit. However, what actually happens to the mass function below about $0.08M_{\odot}$ remains unclear in the galactic disk population. Studies of the halo population, both in globular clusters and the field, suggest that brown dwarfs could be a significant component.

Literally dozens of interesting candidates are being identified and studied further in the Pleiades and Hyades clusters and in the Rho Ophiuchus association. Background problems make membership in the groups somewhat uncertain. There are important uncertainties in (1) the conversion from an observed color to T_e, and in (2) the predictions of the theoretical isochrones of different groups and/or with different physical assumptions. These make it very difficult from the available results to understand whether member objects are brown dwarfs or pre-main-sequence stars of very low mass.

From the systematic programs designed to find companions of substellar mass, a less optimistic working hypothesis has been developed. This hypothesis holds that stars in the local disk population only rarely have companions between about 80 and $10M_{\rm J}$. This conclusion is advanced from the radial velocity surveys of low-mass M stars by Marcy and collaborators, from the more precise velocity measurements of fewer stars of higher mass by Campbell and collaborators, from the infrared speckle work on low-mass solar neighbors by McCarthy and Henry, and from the survey of white dwarfs by Zuckerman and Becklin. It is possible that substantial numbers of companions are formed with masses near, but under, the limit. The most likely substellar objects to have been missed entirely are old, low-mass, and/or very distant companions.

Nevertheless, as should be clear from the extended theoretical discussions in Sec. II and the ample observational survey in Sec. III, the science of brown dwarfs is rich not only with promise, but detail. Since new theoretical spectra and colors will soon be available and infrared technology and surveys are continuing their explosive advance, brown dwarf studies are rapidly joining the other more established branches of stellar astronomy. These substellar objects bridge the realms of planets and stars, may provide the missing mass of the halo, and reside on one of the last scientific frontiers of the astronomical enterprise.

ACKNOWLEDGMENTS

The authors would like to thank F. Allard, and T. Henry, W. Hubbard, J. D. Kirkpatrick, J. Lunine, G. Rieke, D. Saumon for their help during the preparation of this manuscript. A. B. acknowledges the support of the NSF and NASA through Grants AST89-14346 and NAGW-2145, respectively. J. L. acknowledges the support of the NSF through Grant AST89-18471.

REFERENCES

Adams, F. C., and T. P. Walker, 1983, Astrophys. J. **359**, 57.
Alexander, D.R., H. R. Johnson, and R. L. Rypma, 1983, Astrophys. J. **272**, 773.
Allard, F., 1991, Ph.D. thesis (University of Heidelberg).
Bahcall, J. N., 1986, Annu. Rev. Astron. Astrophys. **24**, 577.
Bailes, M., A. G. Lyne, and S. L. Shemar, 1991, Nature **352**, 311.
Barnbaum, C., and B. Zuckerman, 1992, Astrophys. J. Lett. **396**, L31.
Barsony, M., M. G. Burton, A. P. G. Russell, J. E. Carlstrom, and R. P. Garden, 1989, Astrophys. J. Lett. **346**, L93.

Becklin, E. E., and B. Zuckerman, 1988, Nature **336**, 656.
Beichman, C. A., T. Chester, F. C. Gillett, F. J. Low, K. Matthews, and G. Neugebauer, 1990, Astron. J. **99**, 1569.
Berriman, G., and N. Reid, 1987, Mon. Not. R. Astron. Soc. **227**, 315.
Berriman, G., N. Reid, and S. Leggett, 1992, Astrophys. J. Lett. **392**, L31.
Bessel, F. W., 1845, Mon. Not. R. Astron. Soc. **6**, 136.
Bessell, M. S., 1991, Astron. J. **101**, 662.
Boss, A. P., 1986, in *Astrophysics of Brown Dwarfs,* edited by M. C. Kafatos, R. S. Harrington, and S. P. Maran (Cambridge University, Cambridge, England), p. 206.
Boss, A. P., 1987, in *Interstellar Processes,* edited by D. Hollenbach and H. Thronson (Reidel, Dordrecht), p. 321.
Boss, A. P., 1990, Publ. Astron. Soc. Pac. **101**, 767.
Brush, S. G., H. L. Sahlin, and E. Teller, 1966, J. Chem. Phys. **45**, 2101.
Bryja, C., T. J. Jones, R. M. Humphreys, G. Lawrence, R. L. Pennington, and W. Zumach, 1992, Astrophys. J. Lett. **388**, L23.
Burrows, A., W. B. Hubbard, and J. I. Lunine, 1989, Astrophys. J. **345**, 939 (BHL).
Burrows, A., W. B. Hubbard, D. Saumon, and J. I. Lunine, 1993, Astrophys. J. (in press).
Burrows, A., and J. M. Lattimer, 1986, Astrophys. J. **307**, 178.
Cameron, A. G. W., 1988, Annu. Rev. Astron. Astrophys. **26**, 441.
Campbell, B., G. A. H. Walker, and S. Yang, 1988, Astrophys. J. **331**, 902.
Carson, T. R., 1992, Rev. Mexicana Astron. Astrof. **23**, 151.
Carson, T. R., G. Luo, and C. M. Sharp, 1992, Rev. Mexicana Astron. Astrof. **23**, 217.
Ceperly, D., 1986, NATO ASI Series B **186**, 477.
Ceperly, D., and B. Alder, 1986, Science **231**, 555.
Chabrier, G., N. Ashcroft, and H. E. DeWitt, 1992, Nature (in press).
Chandrasekhar, S., 1939, *An Introduction to the Study of Stellar Structure* (Dover, New York).
Clayton, D. D. 1968, *Principles of Stellar Evolution and Nucleosynthesis* (McGraw-Hill, New York).
Cochran, W. D., A. P. Hatzes, and T. J. Hancock, 1991, Astrophys. J. Lett. **380**, L35.
Comeron, F., G. H. Rieke, A. Burrows, and M. J. Rieke, 1993, Astrophys. J. (in press).
Cox, A. N., G. Shaviv, and S. W. Hodson, 1981, Astrophys. J. Lett. **245**, L37.
D'Antona, F., 1986, in *Astrophysics of Brown Dwarfs,* edited by M. C. Kafatos, R. S. Harrington, and S. P. Maran (Cambridge University, Cambridge, England), p. 148.
D'Antona, F., 1987, Astrophys. J. **320**, 653.
D'Antona, F., 1990, in *Physical Processes in Fragmentation and Star Formation,* edited by R. Capuzzo-Dolcetta, C. Chiosi, and D. DiFazio (Kluwer, Dordrecht), p. 367.
D'Antona, F., and I. Mazzitelli, 1985, Astrophys. J. **296**, 502.
D'Antona, F., and I. Mazzitelli, 1986, Astron. Astrophys. **162**, 80.
Davidge, T. J., and P. C. Boeshaar, 1991, Astron. J. **102**, 267.
Dawson, P. C., 1986, Astrophys. J. **311**, 984.
Debye, P., 1912, Ann. Phys. (Lepizig) **39**, 789.
Del Genio, A. D., and K. B. McGratten, 1988, Bull. Am. Astron. Soc. **20**, 868.
DeWitt, H. E., and W. B. Hubbard, 1976, Astrophys. J. **205**, 295.
Dorman, B., L. A. Nelson, and W. Y. Chou, 1989, Astrophys. J. **342**, 1003.
Faulkner, J., B. P. Flannery, and B. Warner, 1972, Astrophys. J. Lett. **175**, L79.
Feynman, R. P., N. Metropolis, and E. Teller, 1949, Phys. Rev. **75**, 1561.
Fich, M., and S. Tremaine, 1991, Annu. Rev. Astron. Astrophys. **29**, 409.
Fienberg, R. T., 1990, Sky and Telescope **80**, 370.
Fontaine, G., H. C. Graboske, Jr., and H. M. Van Horn, 1977, Astrophys. J. Suppl. Ser. **35**, 293.
Forrest, W. J., Z. Ninkov, J. D. Garnett, M. F. Skrutskie, and M. Shure, 1989, in *Third Infrared Detector Technology Workshop,* edited by C. R. McCreight (NASA TM 102209), p. 221.
Forrest, W. J., M. F. Skrutskie, and M. Shure, 1988, Astrophys. J. Lett. **330**, L119.
Fowler, W. A., G. R. Caughlan, and B. A. Zimmerman, 1975, Annu. Rev. Astron. Astrophys. **13**, 69.
Fowler, W. A., and F. Hoyle, 1964, Astrophys. J. Suppl. Ser. **9**, 201.
Fruchter, A. S., J. E. Gunn, T. R. Lauer, and A. Dressler, 1988, Nature **334**, 686.
Gatewood, G., M. Castelaz, I. Han, T. Persinger, J. Stein, B. Stephenson, and W. Tangren, 1990, Astrophys. J. **364**, 114.
Gatewood, G., and H. Eichhorn, 1973, Astron. J. **78**, 769.
Giclas, H. L., 1958, Lowell Obs. Bull. **4**, 1.
Gilmore, G., and N. Reid, 1983, Mon. Not. R. Astron. Soc. **202**, 1025.
Gilmore, G., N. Reid, and P. Hewitt, 1985, Mon. Not. R. Astron. Soc. **213**, 257.
Gliese, W., 1969, *Catalogue of Nearby Stars,* Veröff. Astron. Rechen Inst. Heidelberg, No. 22 (Verlag G. Braun, Karlsruhe).
Gliese,W., 1974, Astron. Astrophys. **34**, 147.
Gould, A., and A. Loeb, 1992, Astrophys. J **396**, 104.
Graboske, H. C., H. E. DeWitt, A. S. Grossman, and M. S. Cooper, 1973, Astrophys. J. **181**, 457.
Graham, J. R., K. Matthews, J. L. Greenstein, G. Neugebauer, C. Tinney, and S. E. Persson, 1992, Astron. J. **104**, 2016.
Graham, J. R., K. Matthews, G. Neugebauer, and B. T. Soifer, 1990, Astrophys. J. **357**, 216.
Graham, J. R., J. K. McCarthy, I. N. Reid, and R. M. Rich, 1990, Astrophys. J. Lett. **357**, L21.
Greenstein, J. L., 1988, Astron. J. **95**, 1494.
Greenstein, J. L., 1989a, Comments Astrophys. **13**, 303.
Greenstein, J. L. 1989b, Publ. Astron. Soc. Pac. **101**, 787.
Griest, K., 1991, Astrophys. J. **366**, 412.
Griest, K., C. Alcock, T. S. Axelrod, D. P. Bennett, K. H. Cook, K. C. Freeman, H.-S. Park, S. Perlmutter, B. A. Peterson, P. J. Quinn, A. W. Rodgers, and C. W. Stubbs (The MACHO Collaboration), 1991, Astrophys. J. Lett. **372**, L79.
Grossman, A. S., 1970, Astrophys. J. **161**, 619.
Grossman, A. S., D. Hays, and H. C. Graboske, 1974, Astron. Astrophys. **30**, 95.
Grüneisen, E., 1926, in *Handbuch der Physik,* edited by H. Greiger and K. Scheel (Springer, Berlin), Vol. 10, p. 1.
Haas, M., and C. Leinert, 1990, Astron. Astrophys. **230**, 87.
Hambly, C. C., M. R. S. Hawkins, and R. F. Jameson, 1991, Mon. Not. R. Astron. Soc. **253**, 1.
Hambly, N. C., and R. F. Jameson, 1991, Mon. Not. R. Astron. Soc. **249**, 137.
Hansen, J. P., 1973, Phys. Rev. A **8**, 3096.
Harrington, R. S., 1986, in *Astrophysics of Brown Dwarfs,* edited by M. C. Kafatos, R. S. Harrington, and S. P. Maran (Cambridge University, Cambridge, England), p. 3.

Hawkins, M. R. S., 1986, Mon. Not. R. Astron. Soc. **223**, 845.
Hawkins, M. R. S., and M. S. Bessell, 1988, Mon. Not. R. Astron. Soc. **234**, 177.
Heintz, W. D., 1978, Astrophys. J. **20**, 931.
Heintz, W. D., 1989, Astron. Astrophys. **217**, 145.
Henry, T. J., 1991, Ph.D. thesis (University of Arizona).
Henry, T. J., D. S. Johnson, D. W. McCarthy, and J. D. Kirkpatrick, 1992, Astron. Astrophys. **254**, 116.
Henry, T. J., and D. Kirkpatrick, 1990, Astrophys. J. Lett. **354**, L29.
Henry, T. J., and D. W. McCarthy, Jr., 1990, Astrophys. J. **350**, 334.
Hubbard, W. B., 1984, *Planetary Interiors* (Van Nostrand Reinhold, New York).
Hubbard, W. B., 1986, in *Astrophysics of Brown Dwarfs,* edited by M. C. Kafatos, R. S. Harrington, and S. P. Maran (Cambridge University, Cambridge, England), p. 160.
Hubbard, W. B., A. Burrows, and J. I. Lunine, 1990, Astrophys. J. Lett. **358**, L53.
Hubbard, W. B., and H. E. DeWitt, 1985, Astrophys. J. **290**, 388.
Ichimaru, S., 1982, Rev. Mod. Phys. **54**, 1017.
Jameson, R. F., M. R. Sherrington, and A. B. Giles, 1983, Mon. Not. R. Astron. Soc. **205**, 39.
Jameson, R. F., and I. Skillen, 1989, Mon. Not. R. Astron. Soc. **239**, 247.
Jarrett, T. H., 1992, Ph.D. dissertation (University of Massachusetts).
Kafatos, M. C., R. S. Harrington, and S. P. Maran, 1986, Eds., *Astrophysics of Brown Dwarfs* (Cambridge University, Cambridge, England), p. 198.
Kirkpatrick, J. D., 1992, Ph.D. dissertation (University of Arizona).
Kirkpatrick, J. D., T. J. Henry, and J. Liebert, 1993, Astrophys. J. (in press).
Kirkpatrick, J. D., T. Henry, and D. McCarthy, Jr., 1991, Astrophys. J. Suppl. Ser. **77**, 417.
Kirkpatrick, J. D., D. M. Kelly, G. H. Rieke, J. Liebert, F. Allard, and R. Wehrse, 1993, Astrophys. J. **402**, 643.
Kleinman, S. G., *et al.*, 1991, proposal to NASA/NSF for a 2 Micron All Sky Survey (2MASS).
Kroupa, P., C. A. Tout, and G. Gilmore, 1990, Mon. Not. R. Astron. Soc. **244**, 76.
Kumar, S., 1963, Astrophys. J. **137**, 1121.
Kumar, S., 1987, Astron. J. **94**, 158.
Latham, D. W., T. Mazeh, R. P. Stefanik, M. Mayor, and G. Burki, 1989, Nature **339**, 38.
Leggett, S. K., and M. R. S. Hawkins, 1988, Mon. Not. R. Astron. Soc. **234**, 1065.
Leggett, S. K., and M. R. S. Hawkins, 1989, Mon. Not. R. Astron. Soc. **238**, 145.
Lenzuni, P., D. Chernoff, and E. E. Salpeter, 1991, Astrophys. J. Suppl. **76**, 759.
Liebert, J., 1991, in *Frontiers of Stellar Evolution,* ASP Conference Series, Vol. 20, edited by D. L. Lambert (ASP, Provo, Utah), p. 125.
Liebert, J., and R. G. Probst, 1987, Annu. Rev. Astron. Astrophys. **25**, 473.
Lippincott, S. L., 1978, Space Sci. Rev. **22**, 153.
Lunine, J. I., 1986, in *Astrophysics of Brown Dwarfs,* edited by M. C. Kafatos, R. S. Harrington, and S. P. Maran (Cambridge University, Cambridge, England), p. 170.
Lunine, J. I., W. B. Hubbard, A. Burrows, Y. P. Wang, and K. Garlow, 1989, Astrophys. J. **338**, 314.
Lunine, J. I., W. B. Hubbard, and M. S. Marley, 1986, Astrophys. J. **310**, 238.
Lunine, J. I., and D. M. Hunten, 1987, Icarus **69**, 566.
Luyten, W. J., 1963, *Proper Motion Survey With the 48-inch Schmidt Telescope,* No. 1 (University of Minnesota, Minneapolis).
Luyten, W. J., 1976, *Proper Motion Survey With the 48-inch Schmidt Telescope,* No. 46 (University of Minnesota, Minneapolis), LHS Catalog, 2nd ed.
Luyten, W. J., 1979a, The LHS Catalogue (University of Minnesota, Minneapolis).
Luyten, W. J., 1979b, The LHS Atlas (University of Minnesota, Minneapolis).
Luyten, W. J., 1979c, The NLTT Catalogue (University of Minnesota, Minneapolis).
Lyne, A. G., R. N. Manchester, N. D'Amico, L. Staveley-Smith, S. Johnston, J. Lim, A. S. Fruchter, W. M. Goss, and D. Frail, 1990, Nature **347**, 650.
Macintosh, B., B. Zuckerman, E. E. Becklin, and I. S. McLean, 1992, Bull. Am. Astron. Soc. **24**, 773.
Magni, G., and I. Mazzitelli, 1979, Astron. Astrophys. **72**, 134.
Mao, H. K., and R. J. Hemley, 1989, Science **244**, 1462.
Mao, H. K., R. J. Hemley, and M. Hanfland, 1990, Phys. Rev. Lett. **65**, 484.
Mao, H. K., and B. Paczynski, 1991, Astrophys. J. Lett. **374**, L37.
Marcy, G. W., and K. J. Benitz, 1989, Astrophys. J. **344**, 441.
Marcy, G. W., and D. Moore, 1988, Astrophys. J. **341**, 961.
Marley, M. S., and W. B. Hubbard, 1988, Icarus **73**, 536.
Marley, M. S., J. I. Lunine, and W. B. Hubbard, 1990, Astrophys. J. Lett. **348**, L37.
Mazeh, T., D. W. Latham, R. D. Mathieu, and B. W. Carney, 1990, in *Active Close Binaries,* edited by C. İbanoğlu (Kluwer Academic, Dordrecht), p. 145.
McCarthy, D. W., Jr., M. L. Cobb, and R. G. Probst, 1987, Astron. J. **93**, 1535.
McCarthy, D. W., Jr., and T. J. Henry, 1987, Astrophys. J. Lett. **319**, L93.
McCarthy, D. W., Jr., T. Henry, T. A. Fleming, R. A. Saffer, J. Liebert, and J. C. Christou, 1988, Astrophys. J. **333**, 943.
McCarthy, D. W., Jr., R. G. Probst, and F. J. Low, 1985, Astrophys. J. Lett. **290**, L9.
McMillan, R. S., 1992, private communiction.
McMillan, R. S., P. H. Smith, J. E. Frecker, W. J. Merline, and M. L. Perry, 1985, in *Stellar Radial Velocities,* Proceedings of IAU Colloquium 86, edited by A. G. Davis Philip and D. W. Latham (L. Davis, Schenectady), p. 63.
Mestel, L., and M. A. Ruderman, 1967, Mon. Not. R. Astron. Soc. **136**, 27.
Mihalas, D., 1978, *Stellar Atmospheres* (Freeman, San Francisco).
Monet, D. G., C. C. Dahn, F. J. Vrba, H. C. Harris, J. R. Pier, C. B. Luginbuhl, and H. D. Ables, 1992, Astron. J **103**, 638.
Nellis, W. J., A. C. Mitchell, M. van Thiel, G. J. Devine, R. J. Trainor, and N. Brown, 1983, J. Chem. Phys. **79**, 1480.
Nelson, L. A., S. A. Rappaport, and P. C. Joss, 1985, Nature **316**, 42.
Nelson, L. A., S. A. Rappaport, and P. C. Joss, 1986a, Astrophys. J. **204**, 231.
Nelson, L. A., S. A. Rappaport, and P. C. Joss, 1986b, Astrophys. J. **311**, 226.
Nelson, L. A., S. A. Rappaport, and P. C. Joss, 1986c, in *Astrophysics of Brown Dwarfs,* edited by M. C. Kafatos, R. S. Har-

rington, and S. P. Maran (Cambridge University, Cambridge, England), p. 177.
Ogata, S., and S. Ichimaru, 1987, Phys. Rev. A **36**, 5451.
Oort, J., 1960, Bull. Astron. Inst. Neth. **15**, 45.
Paczynski, B., 1986, Astrophys. J. **304**, 1.
Paczynski, B., 1991, Astrophys. J. Lett. **371**, L63.
Paczynski, B., and R. Sienkiewicz, 1981, Astrophys. J. Lett. **348**, L27.
Patterson, J., B. Zuckerman, E. E. Becklin, D. J. Tholen, and T. Hawarden, 1991, Astrophys. J. Lett. **374**, 330.
Perrier, C., and J.-M. Mariotti, 1987, Astrophys. J. Lett. **312**, L27.
Phinney, E. S., C. R. Evans, R. D. Blandford, and S. R. Kulkarni, 1988, Nature **333**, 832.
Pollack, J. B., and P. Bodenheimer, 1989, in *Origin and Evolution of Planetary and Satellite Atmospheres,* edited by S. K. Atreya, J. B. Pollack, and M. S. Matthews (University of Arizona, Tucson), p. 564.
Probst, R., and J. Liebert, 1983, Astrophys. J. **274**, 245.
Rappaport, S., and P. C. Joss, 1984, Astrophys. J. 283, 232.
Rappaport, S., P. C. Joss, and R. Webbink, 1982, Astrophys. J. **254**, 616.
Reid, N., 1987, Mon. Not. R. Astron. Soc. **225**, 873.
Reid, N., 1992, Mon. Not. R. Astron. Soc. **257**, 257.
Reid, N., and G. Gilmore, 1981, Mon. Not. R. Astron. Soc. **196**, 15.
Reid, N., and G. Gilmore, 1984, Mon. Not. R. Astron. Soc. **206**, 19.
Richer, H. B., and G. G. Fahlman, 1992, Nature, **358**, 383.
Richer, H. B., G. G. Fahlman, R. Buonanno, F. Fusi Pecci, L. Searle, and I. B. Thompson, 1991, Astrophys. J **381**, 147.
Rieke, G. H., N. M. Ashok, and R. P. Boyle, 1989, Astrophys. J. Lett. **339**, L71.
Rieke, G. H., and M. J. Rieke, 1990, Astrophys. J. Lett. **362**, L21.
Robinson, E. L., W. D. Cochran, and A. W. Shafter, 1990, Astron. J. **99**, 672.
Robnik, M., and W. Kundt, 1983, Astron. Astrophys. **120**, 227.
Ruan, K., 1991, Ph.D. dissertation (The Australian National University, Mt. Stromlo Observatory).
Salpeter, E. E., 1992, Astrophys. J. **393**, 258.
Sanders, R. H., 1990, Astron. Astrophys. Rev. **2**, 1.
Sarazin, C. L., and R. W. O'Connell, 1983, Astrophys. J. **268**, 552.
Saumon, D., 1990, Ph.D. thesis (University of Rochester).
Saumon, D., and G. Chabrier, 1989, Phys. Rev. Lett. **62**, 2397.
Saumon, D., W. B. Hubbard, G. Chabrier, and H. M. Van Horn, 1992, Astrophys. J. **391**, 827.
Saumon, D., J. I. Lunine, W. B. Hubbard, and A. Burrows, 1992, unpublished.
Scalo, J., 1986, Fundam. Cosmic Phys. **11**, 1.
Schneider, D. P., J. L. Greenstein, M. Schmidt, and J. E. Gunn, 1991, Astron. J. **102**, 1180.
Shapiro, S. L., and S. A. Teukolsky, 1983, *Black Holes, White Dwarfs, and Neutron Stars* (Wiley, New York).
Shu, F. H., F. C. Adams, and S. Lizano, 1987, Annu. Rev. Astron. Astrophys. **25**, 23.
Simons, D. A., and E. E. Becklin, 1992, Astrophys. J. **390**, 431.
Skrutskie, M. F., W. J. Forrest, and M. A. Shure, 1986, in *Astrophysics of Brown Dwarfs,* edited by M. C. Kafatos, R. S. Harrington, and S. P. Maran (Cambridge University, Cambridge, England), p. 82.
Skrutskie, M. F., W. J. Forrest, and M. A. Shure, 1987, Astrophys. J. Lett. **312**, L55.
Skrutskie, M. F., W. J. Forrest, and M. Shure, 1989, Astron. J. **98**, 1409.
Slattery, W. L., G. D. Doolen, and H. E. DeWitt, 1982, Phys. Rev. A **26**, 2255.
Spruch, L., 1991, Rev. Mod. Phys. **63**, 151.
Stauffer, J., 1984, Astrophys. J. **280**, 189.
Stauffer, J., D. Hamilton, R. Probst, G. Rieke, and M. Mateo, 1989, Astrophys. J. Lett. **344**, L21.
Stauffer, J., L. W. Hartmann, and D. Latham, 1987, Astrophys. J. Lett. **320**, L51.
Stauffer, J., T. Herter, D. Hamilton, G. H. Rieke, M. J. Rieke, R. Probst, and W. Forrest, 1991, Astrophys. J. Lett. **367**, L23.
Stevenson, D. J. 1976, Phys. Lett. A **58**, 282.
Stevenson, D. J., 1978, Proc. Astron. Soc. Australia **3**, 227.
Stevenson, D. J., 1979, Geophys. Astrophys. Fluid Dyn. **12**, 139.
Stevenson, D. J., 1982, Annu. Rev. Earth Planet. Sci. **10**, 257.
Stevenson, D. J., 1983, Rep. Prog. Phys. **46**, 555.
Stevenson, D. J., 1986, in *Astrophysics of Brown Dwafs,* edited by M. C. Kafatos, R. S. Harrington, and S. P. Maran (Cambridge University, Cambridge, England), p. 218.
Stevenson, D. J., 1991, Annu. Rev. Astron. Astrophys. **29**, 163.
Stevenson, D. J., and N. A. Ashcroft, 1974, Phys. Rev. **A9**, 782.
Stevenson, D. J., and E. E. Salpeter, 1977, Astrophys. J. Suppl. Ser. **35**, 221.
Stringfellow, G., 1986, in *Astrophysics of Brown Dwarfs,* edited by M. C. Kafatos, R. S. Harrington, and S. P. Maran (Cambridge University, Cambridge, England), p. 190.
Stringfellow, G. S., 1991, Astrophys. J. Lett. **375**, L21.
Stringfellow, G. S., D. C. Black, and P. Bodenheimer, 1990, Astrophys. J. Lett. **349**, L59.
Stringfellow, G. S., H. E. DeWitt, and W. L. Slattery, 1990, Phys. Rev. A **41**, 1105.
Tarter, J. C., 1975, Ph.D. thesis (University of California, Berkeley).
Tarter, J. C., 1986, in *Astrophysics of Brown Dwarfs,* edited by M. C. Kafatos, R. S. Harrington, and S. P. Maran (Cambridge University, Cambridge, England), p. 121.
Tinney, C., J. R. Mould, and I. N. Reid, 1992, Astrophys. J. **396**, 173.
Tokunaga, A. T., E. E. Becklin, and B. Zuckerman, 1990, Astrophys. J. Lett. **358**, L21.
Tokunaga, A. T., T. Y. Brooke, E. E. Becklin, and B. Zuckerman, 1990, Bull. Am. Astron. Soc. **22**, 1078.
Tokunaga, A. T., K. W. Hodapp, E. E. Becklin, D. P. Cruickshank, M. Rigler, D. Toomey, R. H. Brown, and B. Zuckerman, 1988, Astrophys. J. Lett. **332**, L71.
Trimble, V., 1987, Annu. Rev. Astron. Astrophys. **25**, 425.
Tsuji, T., 1972, Publ. Astron. Soc. Jpn. **23**, 553.
van Biesbroeck, G., 1961, Astron. J. **51**, 61.
van de Kamp, P., 1977, Vistas Astron. **20**, 501.
van de Kamp, P., 1981, *Stellar Paths* (Reidel, Dordrecht).
van de Kamp, P., 1986, Space Sci. Rev. **43**, 211.
Vandenberg, D. A., and T. J. Bridges, 1984, Astrophys. J. **278**, 679.
Vandenberg, D. A., F. D. A. Hartwick, P. Dawson, and D. R. Alexander, 1983, Astrophys. J. **266**, 747.
Van Horn, H. M., 1991, Science **252**, 384.
Wade, R. A., and K. Horne, 1988, Astrophys. J. **324**, 411.
Whitmire, D. P., J. J. Matese, and L. J. Tomley, 1988, Astron. Astrophys. **203**, 13.
Wigner, E., and H. B. Huntington, 1935, J. Chem. Phys. **3**, 764.
Wilking, B. A., and C. J. Lada, 1983, Astrophys. J. **274**, 698.
Winget, D. E., *et al.*, 1990, Astrophys. J. **357**, 630.

Wolk, S. J., and S. C. Beck, 1990, Publ. Astron. Soc. Pac. **102**, 745.
Zapolsky, H. S., and E. E. Salpeter, 1969, Astrophys. J. **158**, 809.
Zinnecker, H., M. J. McCaughrean, and B. A. Wilking, 1993, in *Protostars and Planets III,* edited by E. Levy and J. I. Lunine (University of Arizona, Tucson), in press.
Zuckerman, B., 1992, in *Planets around Pulsars,* ASP Conference Series Vol. 36, edited J. A. Phillips, S. E. Thorsett, and S. Kulkarni (ASP, Provo, UT), p. 303.
Zuckerman, B., and E. E. Becklin, 1987, Astrophys. J. Lett. **319**, L99.
Zuckerman, B., and E. E. Becklin, 1988, Nature **330**, 138.